JGS
Journal of the Geological Society

Research article

Published online January 6, 2020 https://doi.org/10.1144/jgs2019-052 | Vol. 177 | 2020 | pp. 493–508

Layering and structural inheritance controls on fault zone structure in three dimensions: a case study from the northern Molasse Basin, Switzerland

Vincent Roche[1,2]*, Conrad Childs[1,2], Herfried Madritsch[3] & Giovanni Camanni[1]

[1] Fault Analysis Group, UCD School of Earth Sciences, University College of Dublin, Belfield, Dublin 4, Ireland
[2] Irish Centre for Research in Applied Geosciences, UCD School of Earth Sciences, University College Dublin, Belfield, Dublin 4, Ireland
[3] Nagra, Hardstrasse 73, CH-5430 Wettingen, Switzerland
VR, 0000-0002-9992-7433; CC, 0000-0001-8669-213X; GC, 0000-0001-9690-2583
Present address: GC, DiSTAR, Università degli Studi di Napoli 'Federico II', 80126 Naples, Italy
* Correspondence: vincent.roche@ucd.ie

Abstract: Mechanical heterogeneity of a sedimentary sequence exerts a primary control on the geometry of fault zones and the proportion of offset accommodated by folding. The Wildensbuch Fault Zone in the Swiss Molasse Basin, with a maximum throw of 40 m, intersects a Mesozoic section containing a thick (120 m) clay-dominated unit (Opalinus Clay) over- and underlain by more competent limestone units. Interpretation of a 3D seismic reflection survey indicates that the fault zone formed by upward propagation of an east–west-trending basement structure, through the Mesozoic section, in response to NE–SW Miocene extension. This configuration formed an array of left-stepping normal fault segments above and below the Opalinus Clay. In cross-section a broad monoclinal fold is observed in the Opalinus Clay. Folding, however, is not ubiquitous and occurs in the Opalinus Clay where fault segments above and below are oblique to one another; where they are parallel the fault passes through the Opalinus Clay with little folding. These observations demonstrate that, even in strongly heterogeneous sequences, here a four-fold difference in both Young's modulus and cohesion between layers, the occurrence of folding may depend on the local relationship between fault geometry and applied stress field rather than rheological properties alone.

Received 26 March 2019; **revised** 8 November 2019; **accepted** 13 November 2019

A key control on the geometry and nature of structures formed in response to extensional strains is the mechanical properties of the deformed rocks. This is most evident in sedimentary sequences where, for instance, the mode of fracture (Ferrill & Morris 2003), fracture or fault dip (Peacock & Sanderson 1992; Ferrill *et al.* 2017) and fault displacement gradients (Muraoka & Kamata 1983; Ferrill & Morris 2008; Roche *et al.* 2012) can change across bedding interfaces between lithologies of contrasting competence. Where the competence contrast between interbedded lithologies is large, structures can step or become decoupled across the less competent units so that the sequence of rocks of varying mechanical properties, referred to as the mechanical stratigraphy (Corbett *et al.* 1987; Wilkins & Gross 2002; Laubach *et al.* 2009; Ferrill *et al.* 2017), has a significant impact on the propagation and evolution of extensional faults and fractures (e.g. Peacock & Zhang 1994; Childs *et al.* 1996; Vasquez *et al.* 2018).

The impact of mechanical stratigraphy on extensional faulting is well documented for small faults at outcrop (Peacock & Sanderson 1992; Wilkins & Gross 2002; Ferrill & Morris 2003; Roche *et al.* 2012; Agosta *et al.* 2015) but until the advent of 3D seismic reflection data, studying this relationship in three dimensions was challenging (see Mansfield & Cartwright 1996; Kattenhorn & Pollard 2001). Over the past 10 years there have been many seismic-based studies of the impact of sequence on fault geometry and, in particular, on sequences that contain continuous thick salt units where extensional fault systems are entirely decoupled across the salt layer (Baudon & Cartwright 2008; Jackson & Rotevatn 2013; Tvedt *et al.* 2013; Wilson *et al.* 2013; Lăpădat *et al.* 2017; Deng & McClay 2019). Here we use a 3D seismic reflection survey to examine the impact of a thick (>120 m), clay-dominated, incompetent unit on normal fault geometry.

Displacement across fault zones is accommodated by a combination of discontinuous and continuous deformation, which vary in relative importance over a fault (e.g. Grant & Kattenhorn 2004; Ferrill *et al.* 2011; Childs *et al.* 2017; Delogkos *et al.* 2017; Homberg *et al.* 2017). The continuous component is defined as a change in shape produced by structures that are below the scale of observations. This definition is scale dependent and continuous deformation includes, for example, deformation associated with faulting below the limit of seismic resolution. In contrast, discontinuous deformation is expressed as discrete discontinuities, such as fault offsets. Significant continuous deformation occurs at forced folds above upward propagating normal faults, particularly above less competent units within the faulted sequence (Ferrill *et al.* 2004; Jackson *et al.* 2006; Conneally *et al.* 2017; Lăpădat *et al.* 2017; Roche *et al.* 2017). Continuous deformation also occurs at relay zones between adjacent segments within a segmented fault array that serves to transfer displacement between adjacent segments leading, for example, to relay ramp development between normal faults that overlap one another along-strike (Peacock & Sanderson 1991; Childs *et al.* 1995; Camanni *et al.* 2019). In recent years, a number of seismic-based studies have analysed the variation in discontinuous and continuous deformation (Conneally *et al.* 2017; Lăpădat *et al.* 2017) and demonstrated the complex spatial and temporal variation in the proportion of continuous deformation within fault zones. These and other studies demonstrate that, although the nature of the mechanical sequence is expected to exert a significant control on the distribution of ductile deformation, there are other geometrical controls that are less well understood.

In this paper we describe the geometry and displacement distribution of a normal fault zone that offsets a mechanically heterogeneous sequence in which a thick clay-dominated sequence is under- and overlain by thick carbonate-rich formations. Different parts of the fault zone contrast in the relative importance of continuous deformation and we investigate the likely cause of this variability. In particular, we focus on the control of layering on the continuity of fault segments across the less competent interval, an aspect that is important for general considerations of fault-related fluid conductivity.

Geological setting

Geodynamic evolution

The present study is based on the analysis of a 3D seismic reflection dataset located at the northern margin of the northern Alpine Molasse Basin in Switzerland (Fig. 1). This area has had a polyphase tectonic history (Diebold & Noack 1997; Madritsch 2015; Egli *et al.* 2017, and references therein). The Paleozoic basement, exposed to the north of the study area in the Black Forest Massif of southern Germany (Fig. 1), comprises a variety of crystalline rocks and metasediments deformed during the Late Paleozoic Variscan Orogeny and the following post-collisional extension (Eisbacher *et al.* 1989; Echtler & Chauvet 1992; Geyer *et al.* 2011). The most important basement-rooted fault zones that developed during the extensional stage and affect the study area are the roughly NW–SE-trending Freiburg–Bonndorf–Bodensee Fault zone (Egli *et al.* 2017) and the ENE–WSW-striking Constance–Frick trough, a post-collisional graben system locally associated with several kilometre deep sediment depocentres (Diebold & Noack 1997; Madritsch *et al.* 2018).

The Mesozoic succession overlying the basement was deposited in an epicontintental marine environment (Geyer *et al.* 2011). There are only few and subtle traces of tectonic activity during this depositional phase. However, some researchers have inferred a reactivation of pre-existing faults during Triassic and Early Jurassic times (Wetzel *et al.* 2003; Marchant *et al.* 2005).

The Tertiary was a very active tectonic period, starting with regional uplift in Paleocene–Eocene times related to the development of the Alpine flexural forebulge (Sinclair & Allen 1992; Kempf & Pfiffner 2004). The Central European Rift System, including the Upper Rhine Graben to the west of the study area, developed from the Eocene–Oligocene onwards (Ziegler 1992; Hinsken *et al.* 2007) and was accompanied by regional extension and uplift of the Black Forest Massif in early Miocene times. Contemporaneously, the area of investigation became part of the northern Alpine flexural foreland basin with clastic Molasse deposits being deposited unconformably on top of the Mesozoic sequence (Pfiffner 1986; Sinclair & Allen 1992; Willett & Schlunegger 2010).

The normal faults analysed in this study are related to the so-called Hegau–Lake Constance Graben, located east of the study area (Fig. 1). The activity of this fault system is reported to post-date the early Miocene (Burdigalian) (Schreiner 1992; Hofmann *et al.* 2000), consistent with age data recently derived from U/Pb dating of vein calcite infills in a nearby borehole (Mazurek *et al.* 2018). Its formation is variably interpreted to be due to crustal-scale extension related to the late-stage evolution of the European Rift system (Ziegler 1992; Müller *et al.* 2002) or a deep-seated strike-slip reactivation of the pre-existing Freiburg–Bonndorf–Bodensee Fault zone in relation to Alpine foreland contraction (Egli *et al.* 2017). Extensional strains accommodated by this fault system are low (<1%). A maximum fault throw of 200 m is observed along the Randen Fault NE of the study area (Figs 1 and 2) (Egli *et al.* 2017). Within the study area covered by the 3D seismic survey the most prominent fault belonging to this fault system is the Neuhausen Fault. According to previous subsurface interpretations, its maximum observed throw is *c.* 50 m (Birkhäuser *et al.* 2001). Outcrops reveal further evidence for small-scale normal faults affecting both Late Jurassic and Middle Miocene rocks (Madritsch 2015) (Fig. 2).

The area of investigation lies in the most external part of the Molasse Basin, which, unlike the area to the south, was not decoupled from its basement during Early Miocene Alpine foreland shortening (Burkhard 1990; Jordan *et al.* 2015; Sommaruga *et al.* 2017, and references therein). Alpine contractional deformation is very minor, but a subtle strike-slip overprint of pre-existing structures (with a presumed formation age between Eocene and Middle Miocene) as well as small-scale conjugate strike-slip fault systems are observable in the field (Madritsch 2015; Egli *et al.* 2017).

Stratigraphic succession

Bedrock outcrops are rare within the study area, which is almost entirely covered by unconsolidated Quaternary deposits and a dense vegetation. Nevertheless, the stratigraphic succession is constrained by the Benken borehole (Nagra 2001), which lies at the centre of the analysed seismic survey (Figs 3 and 4). The Benken borehole intersects a crystalline basement horst where Paleozoic gneisses and granites are directly overlain by the Mesozoic sequence. North and south of the study area, Late Paleozoic graben segments are interpreted from 2D and 3D reflection seismic surveys, suggesting that the uppermost Paleozoic section is constituted by Permo-Carboniferous clastic sediments in these areas (Fig. 1) (Marchant *et al.* 2005).

The Mesozoic sedimentary sequence dips gently to the SE (*c.* 5°). Lying on the basal Mesozoic unconformity is the so-called Bundsandstein (Dinkelberg Formation) a metre-thick sandstone overlain by the Middle Triassic Muschelkalk Group. The lower part of the Muschelkalk Group is a roughly 100 m thick succession of marls intercalated with anhydrites and with a layer of rock salt (13 m thick in the Benken borehole; Fig. 3). Its upper part is a *c.* 70 m thick sequence of thick-bedded dolomite and limestone. The Upper Triassic (Keuper Group and Lias) is constituted by marls, intercalated with anhydrites (lower part) and sandstones (upper part). Together, this succession reaches a combined thickness of *c.* 130 m (Jordan *et al.* 2016). It is followed by the Lower to Middle Jurassic Opalinus Clay, a very homogeneous, *c.* 120 m thick claystone. The base of the Opalinus Clay is represented by the very continuous seismic reflection of the Top-Liassic marker horizon (TLi). The rest of the Middle Jurassic section is a *c.* 80 m thick succession of marls intercalated with sand-rich limestone beds (Upper Dogger Group) (compare Nagra 2001, and references therein). The overlying Upper Jurassic sequence (Malm Group) is an up to 250 m thick succession of limestones that has marly intercalation in its middle part but is otherwise dominated by bedded to massive, rheologically stiff rocks. Its top is erosive and karstified, marking a regional unconformity that also represents an important seismic marker horizon (Base-Tertiary).

The Tertiary succession, which unconformably overlies the steeply dipping Mesozoic sequence, comprises clastic sediments of the outermost Alpine Molasse Basin, which forms a wedge with maximum thickness in the SE (*c.* 400 m) and thins out towards the north where the Base-Tertiary crops out (Schreiner 1992; Hofmann *et al.* 2000).

Mechanical stratigraphy

Laboratory tests on samples collected from the Benken borehole combined with wireline logging provide remarkable quantitative insights into the mechanical stratigraphy of the sequence

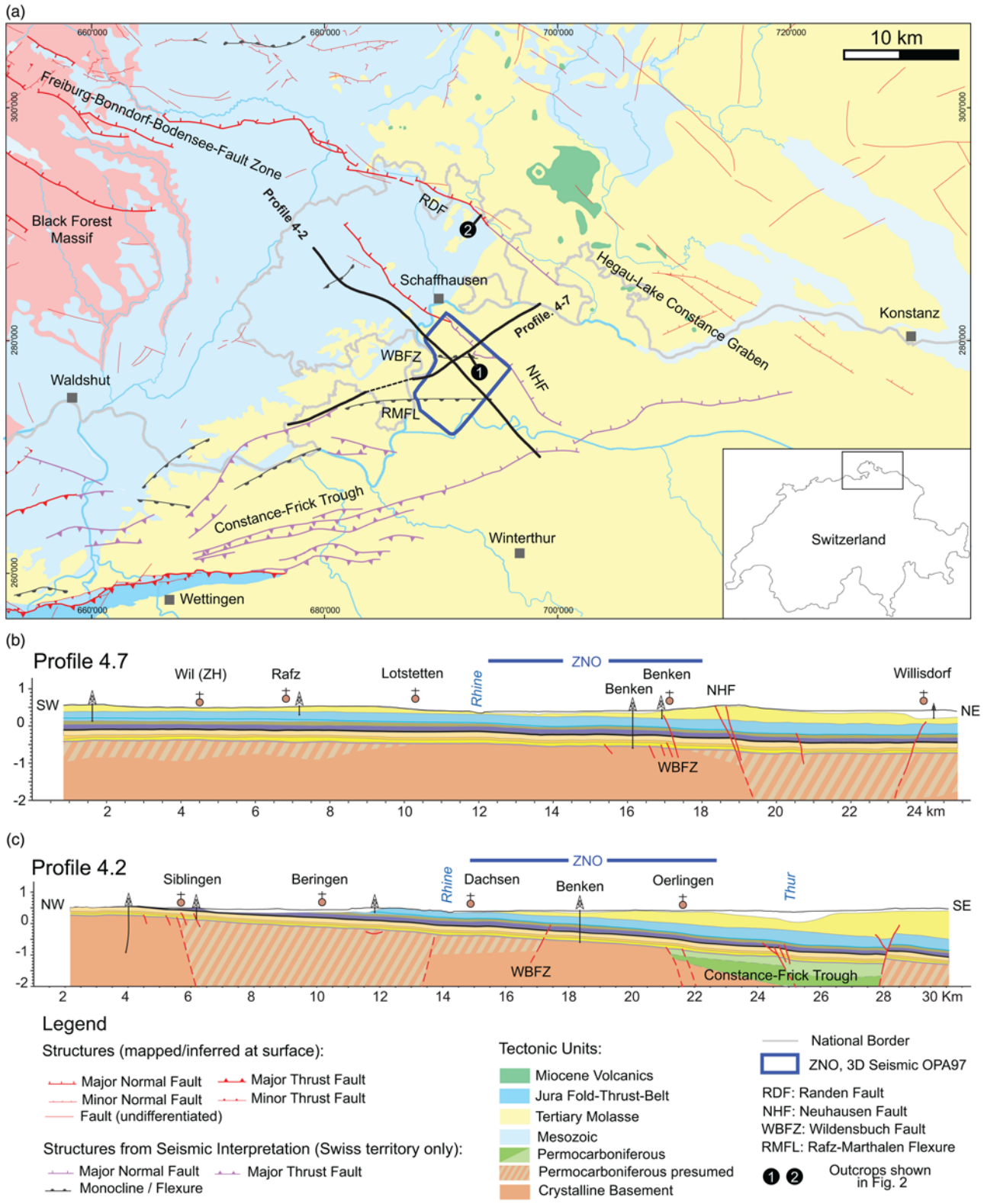

Fig. 1. (**a**) Tectonic map of central northern Switzerland showing the location of the study area (modified after Nagra 2014). (**b**) and (**c**) show profiles 4.7 and 4.2 respectively, modified after Jordan *et al.* (2015).

(Nagra 2001; Giger & Marschall 2014). Rock properties for the different formations encountered in the borehole were calculated from measured P- and S-wave velocities and the density log, which together can be used to assess depth variation in dynamic Young's modulus, using the method presented by Roche & Van der Baan (2015) (Fig. 3). The calculations of Young's modulus were calibrated to the results of a laboratory test programme performed on core plugs sampled from the Benken borehole (Nagra 2001, and references therein), which measured static Young's modulus, cohesion and internal friction. Although a detailed mechanical analysis based on these properties is beyond the scope of this paper these data allow for quantitative comparison between the mechanical properties of the units within the faulted sequence. This indicates that the underlying and overlying Muschelkalk and Malm Groups are significantly stiffer and stronger than the Opalinus Clay, which therefore constitutes a less competent unit between more competent

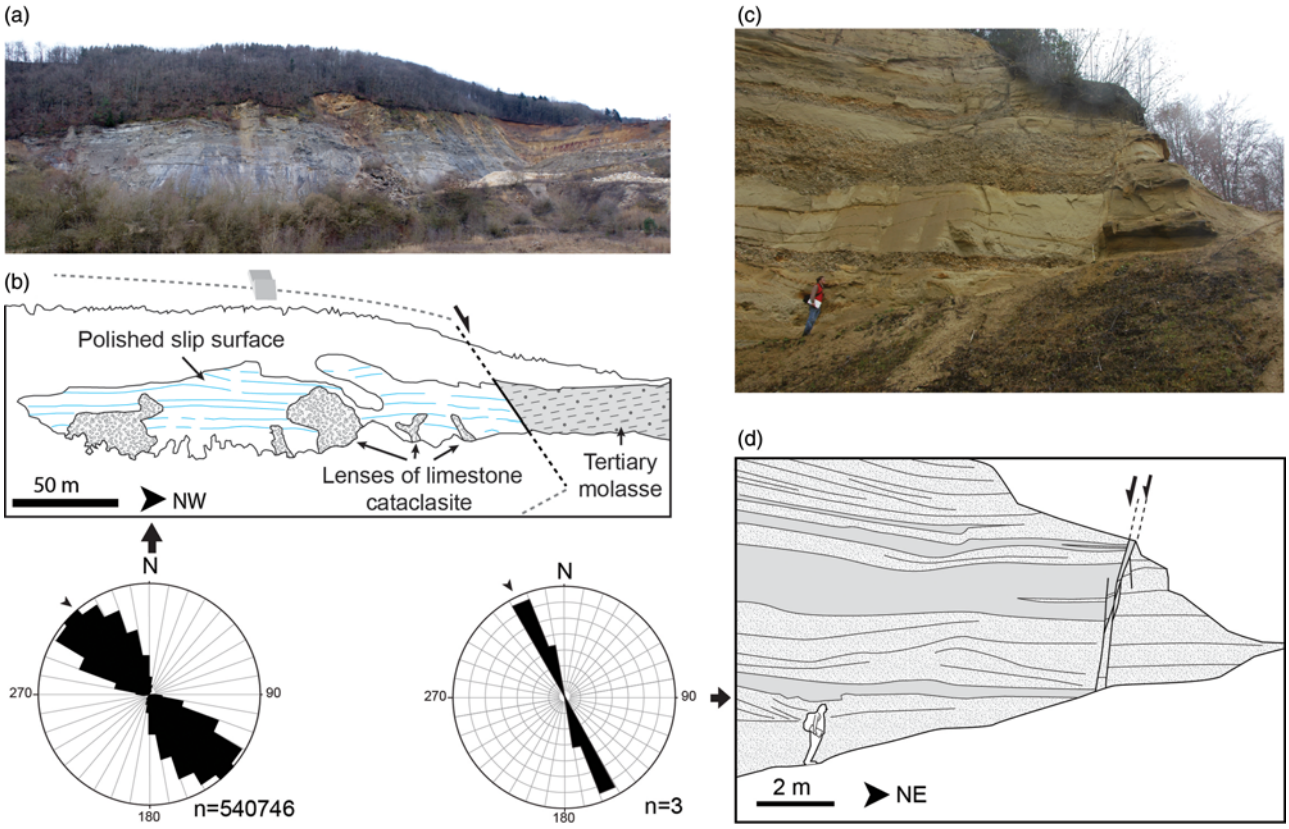

Fig. 2. Examples of normal faults cropping out in the area. (**a**) Panoramic view of the Randen Fault slip surface; corrugations and striations demonstrate normal movements (Egli *et al.* 2017). (**b**) Interpretation and rose diagram showing the strike of the fault. (**c**, **d**) Normal fault in the clastic sediments of the Upper Marine Molasse showing several metres of vertical offset. In the rose diagrams each circle represents 10% of data, the arrowhead represents the average value and the number of data are indicated (mesh elements orientation from photogrammetry in (**b**) and field measurements in (**d**)). Locations of these outcrops are indicated in Figure 1a.

units. The Dogger Group and the Keuper Group are more mixed units. A more detailed analysis of this mechanical stratigraphy and its effect on the faulting is presented in the discussion section.

Seismic data and interpretation

The 3D seismic dataset analysed in this study covers *c.* 50 km^2 and was acquired by the Swiss National Cooperative for Radioactive Waste Disposal (Nagra) in 1997. The initial processing workflow and interpretation has been reported in detail by Birkhäuser *et al.* (2001). Prestack depth migration was carried out later to improve image quality and reduce uncertainty in interpreted fault position. The 3D velocity model needed for this reprocessing was developed iteratively on the basis of a pre-existing regional velocity model that included five Mesozoic intervals (Meier *et al.* 2014), constrained by additional well data and tomographic analysis. Initial results of velocity modelling were calibrated along the Benken borehole (Nagra 2001; see Fig. 4 for location). At the margins of the data cube, regional 2D seismic profiles that were previously depth migrated (compare Meier *et al.* 2014, and references therein) were considered as model control points. Compared with the original legacy dataset the updated prestack depth migration cube has a revised polarity (SEG-inverse EU) and shows a generally increased interpretability (continuity of reflection, homogeneity of amplitude distribution). The seismic interpretation referred to here and illustrated in Figure 4 was done on this reprocessed seismic dataset and may therefore vary slightly from previously published interpretations based on the legacy dataset (Birkhäuser *et al.* 2001; Marchant *et al.* 2005).

Faults were mapped in three dimensions using a combination of inline and crossline interpretation and horizon and seismic attributes. The seismic horizon to well ties were based on synthetic seismograms derived for the Benken borehole (Meier *et al.* 2014) (Fig. 3). Our interpretation of the reprocessed data cube generally agrees with the initial interpretation results of the legacy dataset by Birkhäuser *et al.* (2001), revealing the same overall structural characteristics of the area. The Mesozoic sequence dips gently towards the SSE with a wedge of the Cenozoic Molasse deposits thickening continuously in the same direction. The most important fault recognized in the study area is the Neuhausen Fault imaged in the northeastern part of the seismic cube (Fig. 4). This normal fault is related to the Miocene evolution of the previously mentioned Freiburg–Bonndorf–Bodensee Fault zone (Egli *et al.* 2017). Another deformation zone, referred to as 'Strukturzone von Niderholz' by Birkhäuser *et al.* (2001), is located in the SW of the survey area. It is constituted by a complex array of minor faults ascribed to a Triassic rifting event by Marchant *et al.* (2005) and was not interpreted in detail during this investigation. The interpretation of the Base-Mesozoic marker horizon reveals an east–west crystalline horst structure in the central part of the survey area that separates Late Paleozoic graben elements of the Post-Variscan Constance–Frick trough system (compare Marchant *et al.* 2005; Madritsch *et al.* 2018). The southern and northern border faults of this feature, referred to as the Benken Horst, were apparently reactivated in post-Paleozoic times and are associated with two more deformation zones in the overlying sedimentary sequence. The Rafz–Marthalen flexure occurs at the southern border of the Benken Horst and is characterized by a gentle east–west-trending monocline underlain by a number of similar-striking faults that extend from the basement structure into the Mesozoic sequence (Figs 1 and 4). In the north, the Wildensbuch Fault Zone ('Wildensbuch flexure' of Birkhäuser *et al.* 2001 and Marchant

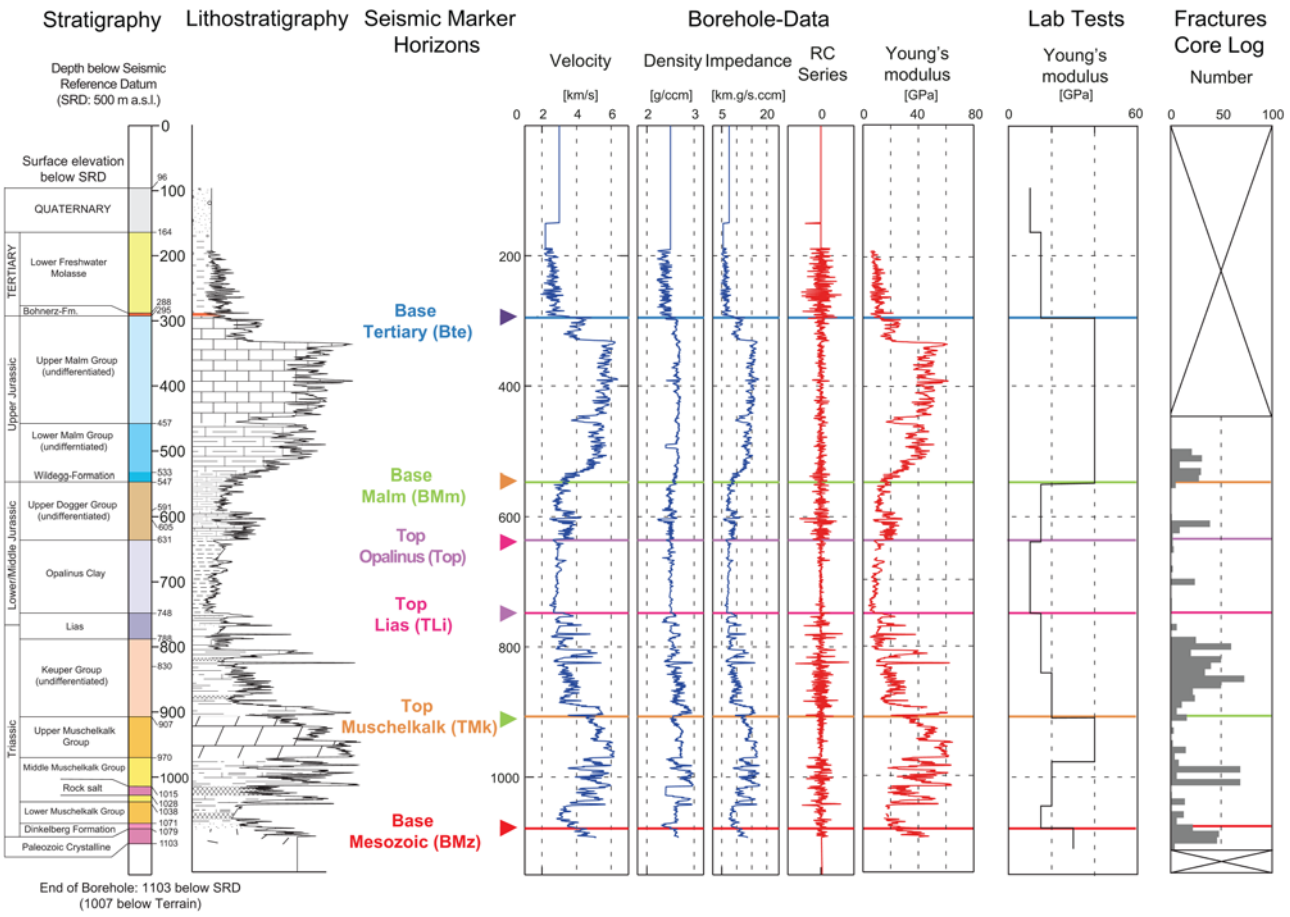

Fig. 3. Stratigraphic sequence recorded in the Benken borehole (location shown in Fig. 4). From left to right: stratigraphy, lithostratigraphy, some of the main horizons identified in the seismic cube, P-wave velocities, density, impedance and RC series. Young's modulus is calculated from the variation in density and velocity. The Young's modulus from laboratory tests is an average value derived from tests on samples collected in the borehole in different intervals (Nagra 2001; Giger & Marschall 2014). Finally, a simplified fracture core log is indicated.

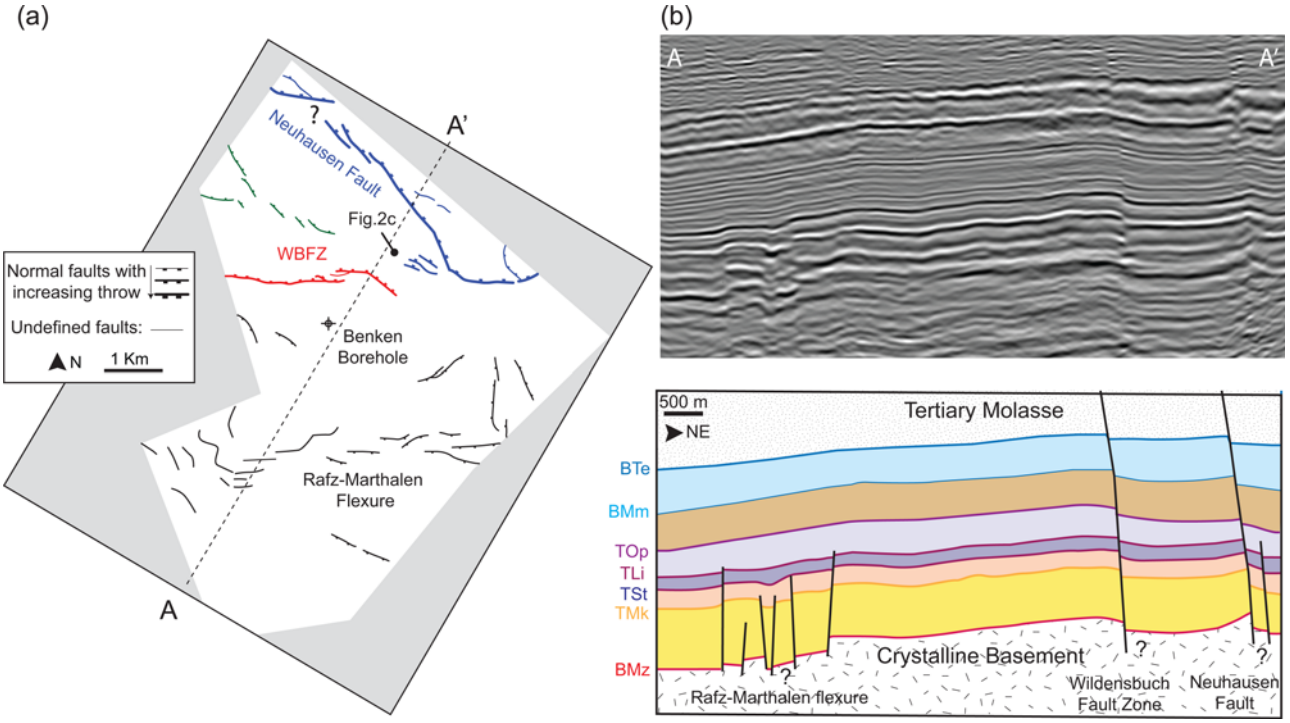

Fig. 4. (**a**) Simplified structural overview showing the main seismically imaged structures in the Muschelkalk. (**b**) A representative seismic section and interpretation along the profile AA' indicated in (**a**) with a vertical exaggeration of ×3.

et al. 2005) is characterized by a series of east–west-trending en echelon fault segments that occasionally extend from the basement up into the Molasse deposits. A more detailed structural characterization of this complex fault zone was the main focus of this study and is presented in the following section.

The Wildensbuch Fault Zone

Field outcrops of the Wildensbuch Fault Zone are very scarce. Its geometry is entirely constrained by interpretation of 3D seismic data. Accordingly, it has a complex 3D structure with strain partitioned between discontinuous deformation accommodated by a system of interacting fault segments and continuous deformation (i.e. folding). As will be demonstrated, partitioning of strain in three dimensions is strongly controlled by the sedimentary layering. In the following sections we first describe the 3D arrangement of the fault segments based on 3D seismic data with a series of maps (Fig. 5), seismic attributes (Fig. 6), a strike projection of the fault surface (Fig. 7) and 3D views of faulted horizons (Fig. 8). We next analyse the orientation of the segments and the partitioning between continuous and discontinuous deformations based on along-strike and down-dip displacement profiles (Figs 9 and 10). In the final section, we broaden the analysis using data from the nearby Neuhausen Fault.

3D segmentation

The geometry of the Wildensbuch Fault Zone varies through the Mesozoic section. From the Base-Mesozoic to the Top-Lias the Wildensbuch Fault Zone consists of two main segments referred to as segment A and segment B (Fig. 5c). These left-stepping segments interact via a relay zone that is most readily mapped at the Base-Mesozoic level and can be seen in a map of seismic coherence at this level (Fig. 6a). Minor fault segments, labelled C and D in Figure 5, have been mapped between segments A and B, but these do not transect the relay zone, which is therefore considered to be intact. The maximum throw on fault segments A and B at the Base-Mesozoic is 40 m (Fig. 9d). These two segments tip-out upwards on the majority of the seismic lines within the Top-Muschelkalk (20%) or the Top-Lias (60%) (Fig. 7a); however, parts of segments A and

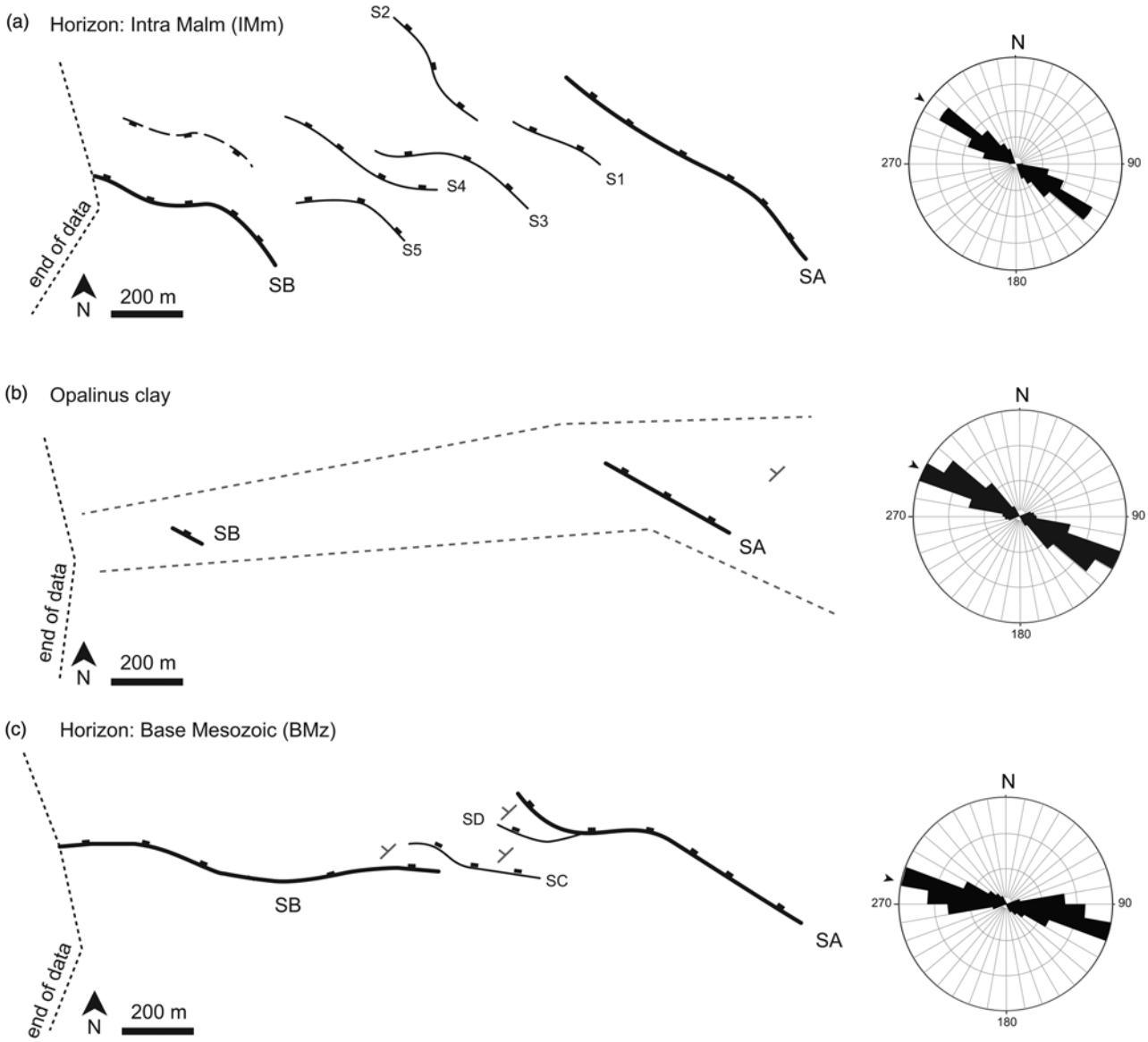

Fig. 5. Fault trace maps of the Wildensbuch Fault Zone in the Malm (IMm) (**a**), the Opalinus Clay (**b**) and the Base-Mesozoic formations (BMz) (**c**). In the rose diagrams of fault strike each circle represents 10% of data and the arrow represents the average value. The strike data correspond to the strike measured on areas of the fault surfaces above the Opalinus Clay (**a**), in the Opalinus Clay (**b**), and below the Opalinus Clay (**c**). SA–SD and S1–S5 refer to the distinct fault segments as discussed in the text.

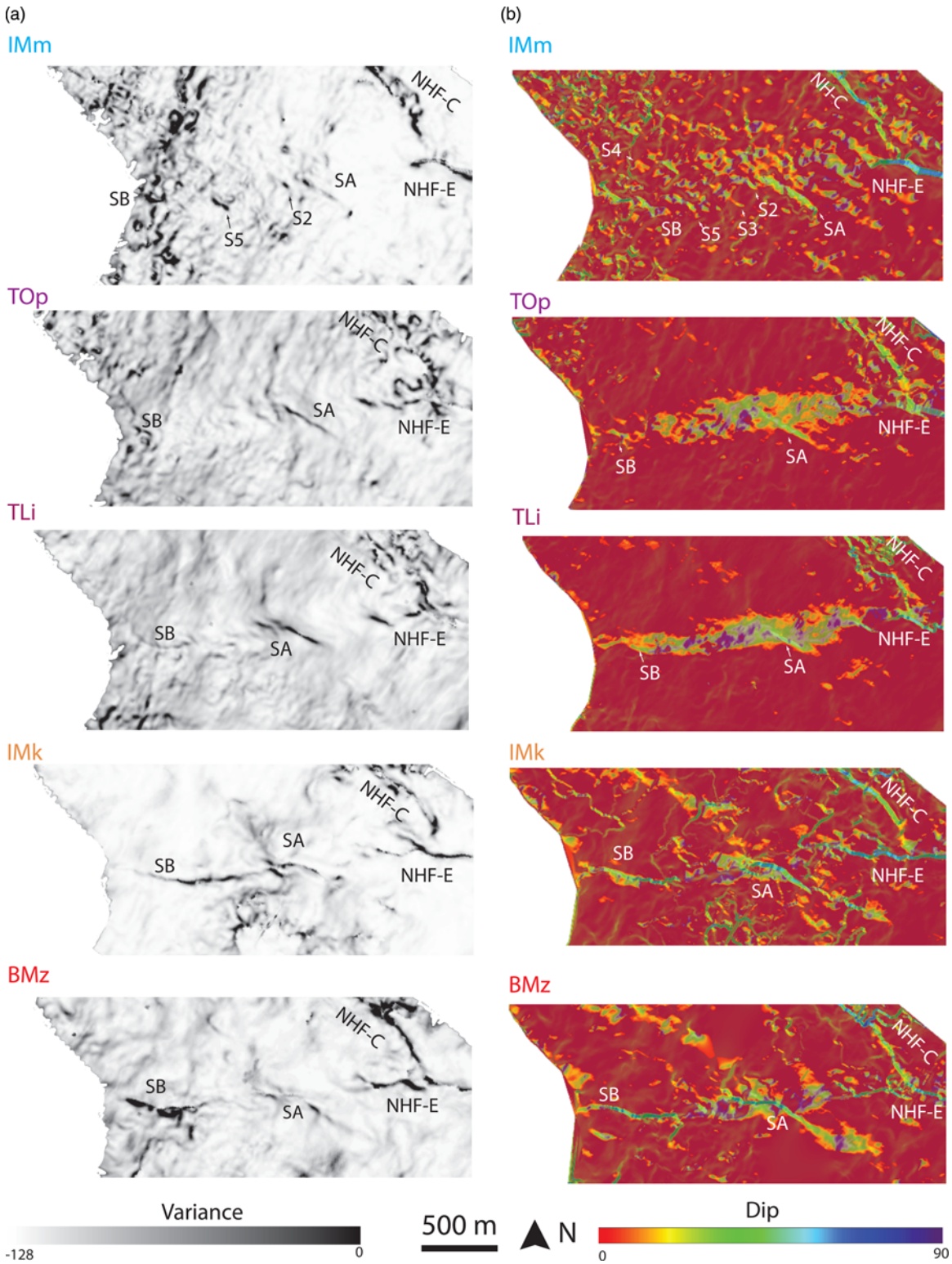

Fig. 6. (**a**) Seismic variance attribute map and (**b**) horizon dip at the Malm (IMm), at the Top-Opalinus (TOp), at the Top-Lias (TLi), in the Muschelkalk (IMk) and at the Base-Mesozoic (BMz). SA, SB, S2, S3, S4 and S5 indicate the location of the fault segments labelled in Figure 5. NHF-E and NHF-C indicate the eastern and the central segments of the Neuhausen Fault labelled in Figure 11. Variance attribute is a measure of the trace-to-trace similarity of waveforms and is commonly used to image discontinuities in seismic data such as at a fault (e.g. Saqab & Bourget 2015).

B are readily mapped across the Opalinus Clay and are continuous from the Base-Mesozoic up to the Malm. Locally, the upper tip of segment B bifurcates upwards to form a series of poorly resolved small left-stepping relay zones (Bi. in Fig. 7a).

In the Jurassic section above the Opalinus Clay, the upper part of the Wildensbuch Fault Zone consists of a left-stepping en echelon array of fault segments (Fig. 5a). The two largest segments within the array, with maximum throws of 20–30 m, are located at the eastern and western extremities of the structure; these segments connect downwards to segments A and B mapped in the lower parts of the Mesozoic section (Figs 5–7 and 9). Between those segments, several smaller faults with throws of 10 m or less are seen on seismic sections (Fig. 7, Section (2)) but unlike the larger faults are not easily identifiable on seismic coherence maps (Fig. 6a). Unlike

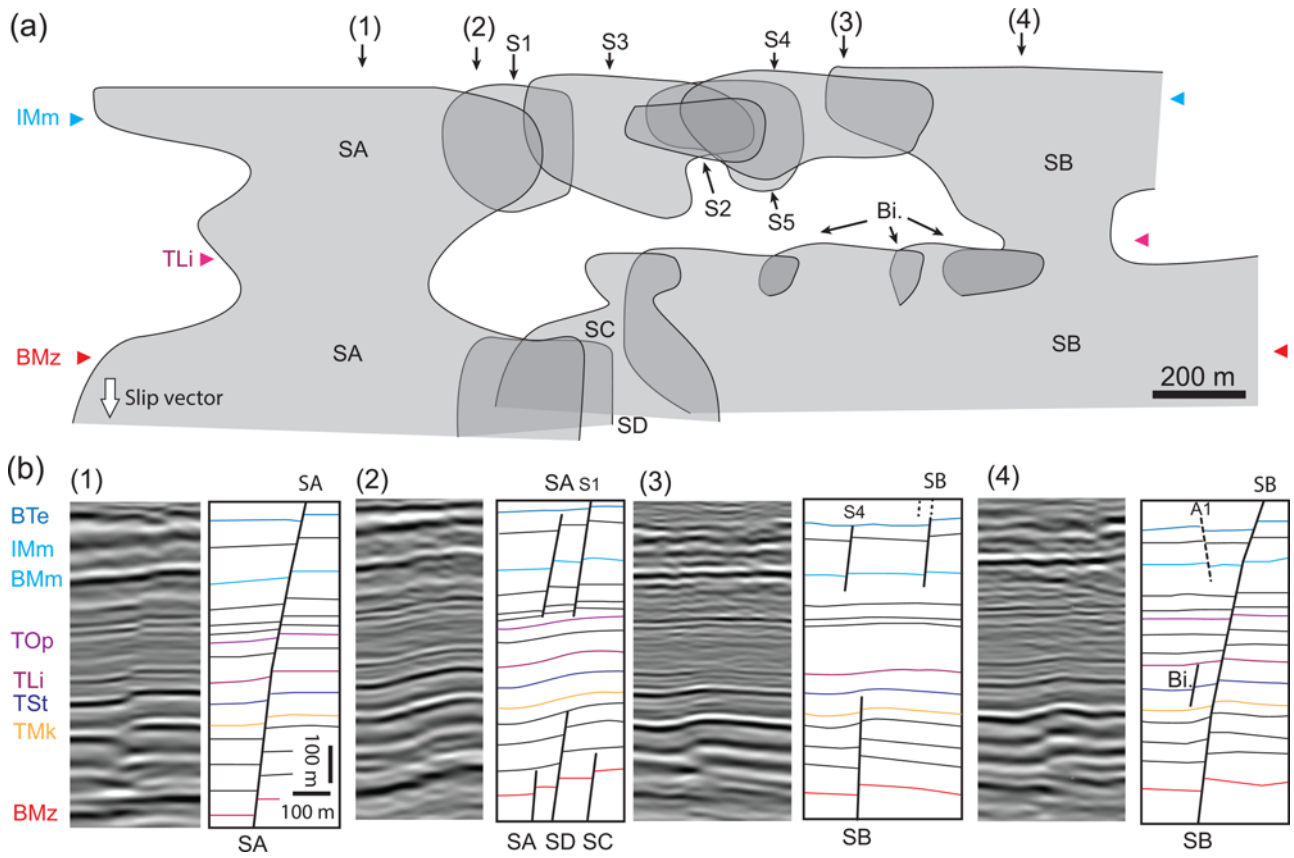

Fig. 7. (**a**) Strike projection of the Wildensbuch Fault Zone. The fault surfaces are represented in grey and fine black lines represent tip-lines. (**b**) Four seismic sections and their interpretation at the locations indicated in (**a**). The colour coding and the terminology for the horizon are as in Figure 3. The segment names are as in Figure 5. Bi. indicates small fault bifurcations.

segments A and B these smaller faults cannot be traced across the Opalinus Clay but tip-out downwards within the Upper Dogger or the Opalinus Clay formations. Most of the faults mapped in the Upper Mesozoic section offset the Base-Tertiary and extend into the Tertiary Molasse, confirming that the faulting is of at least Early Miocene age, which is in line with the previously established regional tectonic history (Schreiner 1992; Madritsch 2015; Egli *et al.* 2017). The upper tips of the fault segments are difficult to define because of the lack of reliable reflectors in this unit but small faults currently exposed at surface are associated with the studied structures (Fig. 2).

Finally, in the middle of the Mesozoic sedimentary sequence, constituted by the Lias and the Opalinus Clay intervals, we do not observe significant faulting along the Wildensbuch Fault Zone. The exceptions are segments A and B, which are present above and below the Opalinus Clay and are locally continuous through the

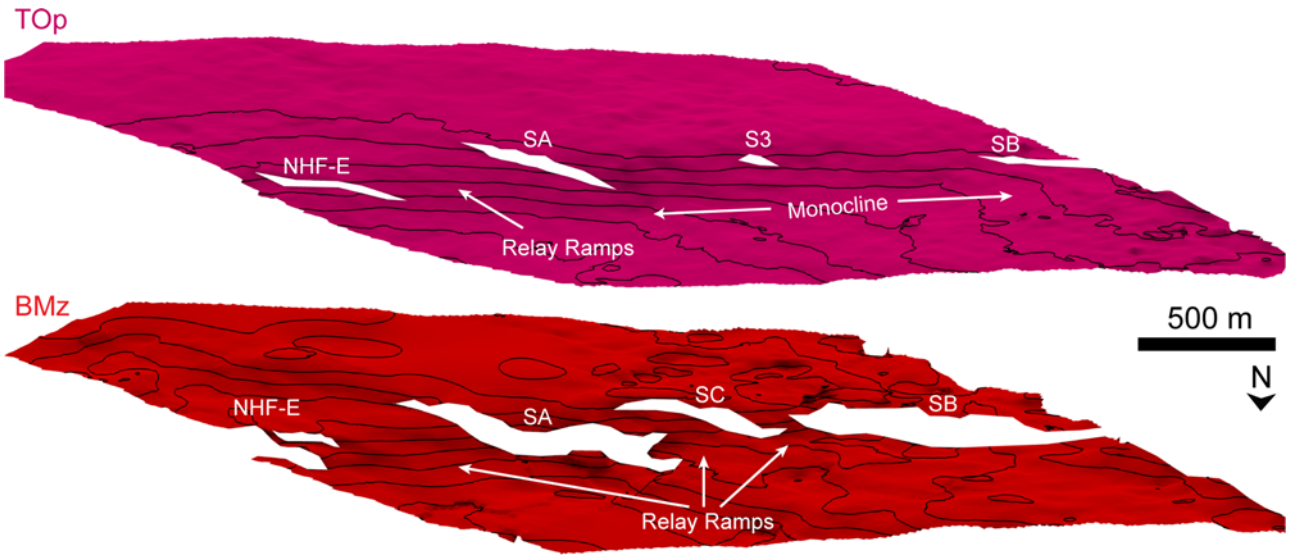

Fig. 8. A 3D view of two horizons centred on the Wildensbuch Fault Zone. The horizons have been rotated along a horizontal axis to remove the regional SE tilt and highlight the local deformation. The fine lines correspond to depth contours of 10 m. The vertical exaggeration is ×3. The names of the segments are as in Figures 5 and 11.

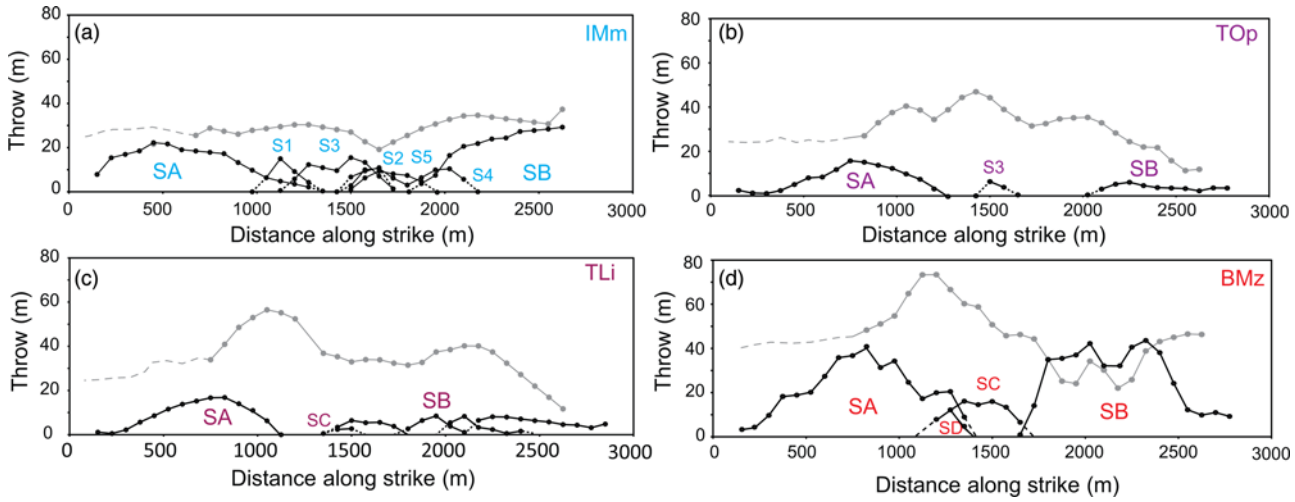

Fig. 9. East–west along-strike displacement profiles in the Malm (**a**), the Top-Opalinus (**b**), the Top-Lias (**c**) and the Base-Mesozoic (**d**). Black, discrete throw; grey, total throw (i.e. discrete throw plus continuous deformation). The total throw profiles are calculated using a trim distance of 300 m on each side of the fault (see text). The uncertainty in throw is *c.* 10 m. The colour coding and labels are as in Figures 3 and 5.

entire section (Figs 5 and 6 and sections (1) and (4) in Fig. 7b). Where discrete throws are mapped within the Opalinus Clay (e.g. section (1) in Fig. 7b) they are lower than the throw on both the over- and underlying Malm and the Muschelkalk intervals (Figs 9 and 10). This locally low value in throw could potentially indicate linkage between initially unconnected upper segments in the Malm and lower segments in Muschelkalk throughout the Opalinus Clay. However, there is no clear evidence to support this conclusion as no overlapping areas are observed that would confirm the earlier existence of down-dip relay zones. Therefore, there is a region in the centre of the Wildensbuch Fault Zone at the level of the Opalinus Clay where the mapped throws are reduced and locally absent, resulting in a hole within the 3D fault surface (Fig. 7), where fault offset is accommodated by folding.

It is possible to locally map segments of the Wildensbuch Fault Zone and their throws below the Base-Mesozoic into the Paleozoic basement. Seismic interpretation at these levels is challenging and is not presented here. As described above, and discussed in previous sections, previous work has identified the presence of a deep-seated northward dipping Paleozoic normal fault (Marchant *et al.* 2005), which underlies the Wildensbuch Fault Zone and probably acted as the locus for its formation.

Fault strike

Vertical variations in the structure of the Wildensbuch Fault Zone are accompanied by changes in the strike of the component fault segments. In the lower part of the fault, in the Muschelkalk interval, fault segments strike 105° on average (Fig. 5c). In the upper part of the fault, in the Malm interval, the en echelon fault segments strike on average 125° (Fig. 5a), with significant variability in fault strike along the segments with notably few portions striking more east–west; for instance, along segments B, 5 and 3 in Figure 5a. The two fault segments within the Opalinus Clay strike 110° on average, which is an intermediate value between the averages obtained for the Muschelkalk and the Malm intervals. This rotation in fault strike with depth, together with the en echelon trace map pattern are typical of oblique reactivation of a pre-existing basement structure (Grant & Kattenhorn 2004; Giba *et al.* 2012; Worthington & Walsh 2017). This hypothesis is discussed below.

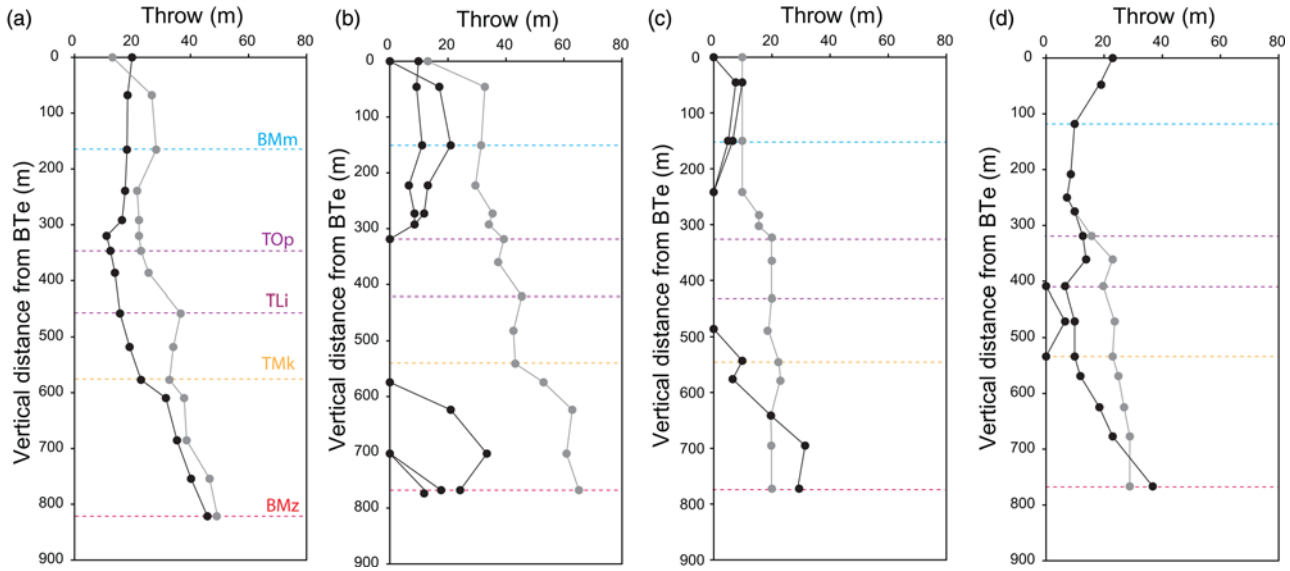

Fig. 10. (**a**–**d**) Down-dip throw profiles for the four sections illustrated in Figure 7. Line styles are as in Figure 9. The vertical distance is counted positive downward from the Base-Tertiary horizon (BTe).

Continuous and discontinuous deformation

Continuous deformation occurs within relay zones allowing transfer of displacement between fault segments. In bedded sequences this continuous deformation is expressed as ramps of elevated bed dip between the relay bounding faults. Relay ramps are difficult to identify where (1) layer dips in the relay ramp are low (i.e. displacement gradients on the bounding faults are low), and (2) where the spacing between the relay ramp-bounding faults is very large or very small. Case (1) occurs for many segment boundaries in the Wildensbuch Fault Zone where throws are <40 m. However, the largest relay zones, for example, the one between fault segments A and B within the Muschelkalk (Fig. 8), are readily mapped.

In addition to relay zones between fault segments, continuous deformation within the Wildensbuch Fault Zone occurs as synthetic dip in the footwall and/or the hanging wall of the discrete faults (see Ferrill *et al.* 2005) and as open monoclines without any resolvable faults (see Conneally *et al.* 2017). This deformation is clearly visible in cross-section (Fig. 7b) and its distribution can be observed on horizon dip maps (Fig. 6b). Monoclinal folding is most notably developed within the Opalinus Clay, where a continuous monoclinal limb is up to 300 m wide. In the upper and lower parts of the fault zone, in the Malm and Muschelkalk formations respectively, folding is more restricted and is focused between the fault segments. Continuous deformation progressively diminishes to the west towards the tip of the Wildensbuch Fault Zone. However, a broad monocline also occurs between segment A and the Neuhausen Fault toward the west, indicating transfer of displacement between these faults (Fig. 8).

The total throw across the Wildensbuch Fault Zone is measured as the vertical difference between two along-strike profiles of horizon elevation drawn on the upthrown and downthrown sides of the zone at the outer limits of deformation. Profiles of total throw measured in this way along-strike and down-dip are shown in Figures 9 and 10, respectively. The magnitude of the continuous component of throw can be estimated by the difference between the total throw and the discrete throw represented by the profiles of fault throw. Although there is a degree of subjectivity in measurement of absolute values for the total offset across the Wildensbuch Fault Zone (for instance, owing to the Mesozoic succession's regional dip), we consider that the estimated relative contributions of continuous and discontinuous deformation are robust. Our estimates of total throw are locally slightly lower than the discontinuous throw. This situation arises where reflections are rotated slightly counter to the fault dip direction either as a result of the very low regional dip or between adjacent faults. These minor errors are not corrected to avoid introducing additional measurement subjectivity.

Displacement profiles along fault strike (Fig. 9) and selected down-dip profiles (Fig. 10) demonstrate that continuous deformation makes a relatively minor contribution to the total throw in the upper (Malm and Dogger units, Fig. 9a) and lower (i.e. the Triassic Muschelkalk unit, Fig. 9d) parts of the faulted section whereas there is significant folding within the Opalinus Clay. The contribution of continuous deformation varies over the fault surface; in the Opalinus Clay the contribution is generally over 60% but locally 100% of the total throw whereas above and below the contribution is generally *c.* 20%. The highest percentages are observed in the central part of the Wildensbuch Fault Zone.

The profiles of throw show that the Opalinus Clay is prone to deforming in a continuous manner with the development of open monoclinal folding. Across the Malm and the Muschelkalk intervals deformation is predominantly by discrete faulting and continuous deformation is largely associated with relay zones between fault segments. It is apparent that lithology is the primary control on the relative importance of continuous deformation; however, there is significant along-strike variability as demonstrated by comparison between the seismic lines shown in Figure 7b and the associated throw profiles (Fig. 10). In section (1) in Figure 7b there is a continuous fault cutting through the entire section, including the Opalinus Clay, whereas in section (2) in Figure 7b, 200 m to the west, there are no discrete faults imaged and the throw is accommodated entirely by folding. This lateral variability indicates a second control on the occurrence of continuous deformation. To investigate this secondary control we compare the throw distribution in the Wildensbuch Fault Zone with the nearby Neuhausen Fault.

The Neuhausen Fault

The Neuhausen Fault (Fig. 4) lies close to the northeastern limit of the seismic cube so that parts of the fault are not well imaged. Those parts of the fault that are well imaged (e.g. Fig. 11) provide a useful comparison with the Wildensbuch Fault Zone as the two fault zones share the same geological setting and formed during Miocene extension (Birkhäuser *et al.* 2001; Madritsch 2015; Egli *et al.* 2017). The Neuhausen Fault is composed of three main segments, referred to here as the Neuhausen Fault's western, central and eastern segments (Fig. 11). The Neuhausen Fault's western segment, close to the edge of the data, is poorly imaged and is not further studied here. The central and eastern segments strike NW–SE and east–west, respectively. Regional mapping shows that the overall trend of the Neuhausen Fault is NW–SE and parallel to the larger Randen Fault (Figs 1 and 2). Consequently, the Neuhausen Fault's eastern segment represents a dog-leg in the main fault trace (Fig. 1). Despite their difference in strike, these two segments are clearly elements of the same fault and the continuity in their displacements along the mapped length indicates that they formed at the same time. The Wildensbuch Fault Zone appears as an along-strike continuation of the eastern segment and follows the east–west trend parallel to the inferred basement structure (Marchant *et al.* 2005). The Wildensbuch Fault Zone can be mapped to the kink at the junction between the Neuhausen Fault's central and eastern segments, again indicating that it is kinematically related to the Neuhausen Fault.

Figure 11 shows examples of seismic sections and down-dip displacement profiles across the Neuhausen Fault. Within the seismic survey it has a generally higher throw than the Wildensbuch Fault Zone; that is, about 60 m on average and locally exceeding 100 m. The upper end of this range is higher than previous estimates based on seismic interpretations in the time domain (Birkhäuser *et al.* 2001). The profiles show a slight downward decrease in throw across the Neuhausen Fault's eastern segment (Fig. 11c and d) and a slight downward increase in throw on its central segment (Fig. 11e and f). In all sections, the fault is continuous across the Mesozoic section including the Opalinus Clay and the pronounced monocline development seen in the Wildensbuch Fault Zone is absent on the Neuhausen Fault. There are, however, more subtle expressions of the impact of the Opalinus Clay on fault geometry and throw distribution. For example, there is a slight decrease in the discontinuous components of throw, observable in the displacement profiles (see Fig. 11), and also a local change in fault dip at the base of the Opalinus Clay (Top-Liassic), with higher dips in the lower portion of the sequence than in the upper portion. This refraction could be due to a change in friction angle, a change in failure mode, or linkage between earlier formed steep segments across a dip relay zone (for review, see Ferrill *et al.* 2017). Irrespective of origin, refracted fault traces reflect a sediment layering control on fault geometry.

Fault geometric control on continuous deformation

The Wildensbuch Fault Zone displays significant variability in fault strike above and below the Opalinus Clay. This is not a feature of the

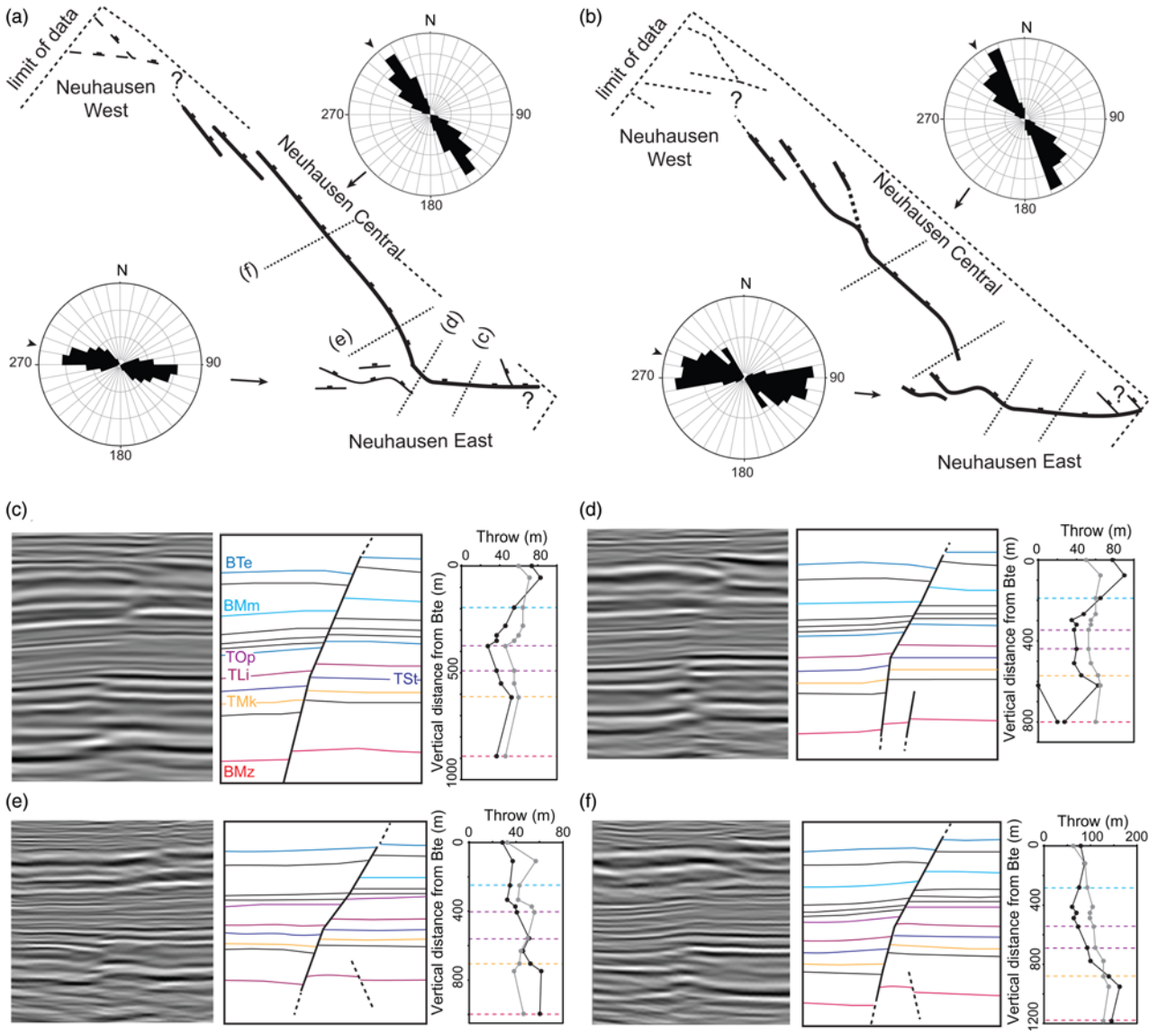

Fig. 11. (**a**, **b**) Maps of the Neuhausen Fault showing the main fault segments observed below and above the Opalinus Clay, respectively. (**c**–**f**) Examples of sections and down-dip throw profiles for the Neuhausen Fault showing no strong evidence of segmentation down fault dip. Line styles, colours coding and labels are as in Figures 3, 5 and 9.

Neuhausen Fault, on which, despite the difference in strike between the Neuhausen Fault's central and eastern segments, the fault traces mapped on the Muschelkalk and Malm horizons have the same strike. This difference between the two faults is represented in a cross-plot of fault strike above and below the Opalinus Clay measured on selected representative sections (Fig. 12a). The measured difference in the strike of faults above and below the Opalinus Clay (angle β) for both the Wildensbuch Fault Zone and the Neuhausen Fault is positively correlated with the proportion of throw accommodated by continuous deformation within the Opalinus Clay (Fig. 12b). This illustrates that the larger the mismatch in throw across the Opalinus Clay, the greater is the proportion of continuous deformation. This relationship is defined primarily by datapoints derived from the Wildensbuch Fault Zone and is consistent with the observation that the two areas where the Wildensbuch Fault Zone forms a continuous fault surface across the Opalinus Clay with limited folding are those where the strikes of faults in the Muschelkalk and the Malm intervals are parallel at *c.* 120° (compare Fig. 5a and c). These observations indicate that there is a relationship between fault geometry and the proportion of continuous deformation within the Opalinus Clay and that, although this relatively weaker lithology is more prone to continuous deformation than other parts of the sequence, significant continuous deformation occurs only in certain geometrical circumstances. The distribution of continuous deformation in sections above and below the Opalinus Clay is largely controlled by the locations of relay zones so that there is no relationship between β and the magnitude of continuous deformation within these levels (Fig. 12c).

Discussion

Comparison between fault geometry and mechanical stratigraphy

Rheological sequence has been identified as a primary control on the occurrence of continuous deformation within fault zones on a range of scales from outcrop to seismic scale (e.g. Jackson *et al.* 2006; Ferrill *et al.* 2017; Lăpădat *et al.* 2017; Deng & McClay 2019); however, the actual mechanical properties of the sequence are rarely reported (Morris *et al.* 2009; Roche *et al.* 2014; Ferrill *et al.* 2017), particularly at the large scale studied here. An extensive programme of laboratory tests on samples collected from the Benken borehole in the centre of the study area (Nagra 2001; Giger & Marschall 2014) provides the data with which to constrain the

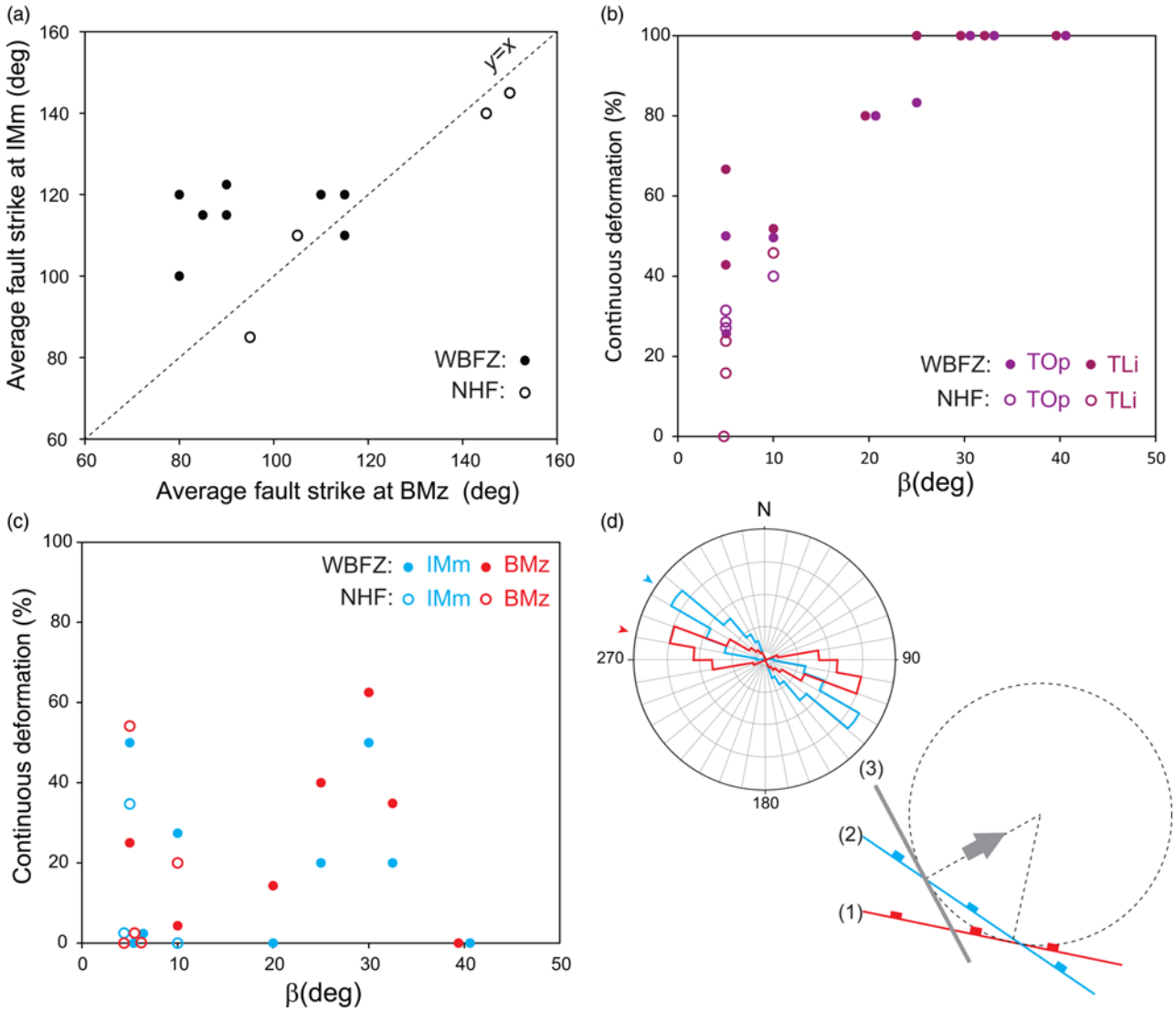

Fig. 12. (**a**) Plot of average fault strike at the Malm (IMm) v. average fault strike at the Base-Mesozoic (BMz) of selected locations along the Wildensbuch Fault Zone (WBFZ) and the Neuhausen Fault (NHF). (**b**, **c**) Plots of continuous deformation expressed as a percentage of the total throw v. β at the Top-Opalinus (TOp) and the Top-Lias (TLi) levels (**b**), and at the Malm (IMm) and Base-Mesozoic (BMz) levels (**c**). The β angle is the difference between the local strikes of the fault in the Malm and at the Base-Mesozoic levels. (**d**) Rose diagrams showing fault strike below (red) and above (blue) the Opalinus Clay and the McCoss construction for the Wildensbuch Fault Zone (McCoss 1986). The orientations (1) and (2) correspond to the average orientations of the fault zone below and above the Opalinus Clay, respectively. The grey arrow indicates the direction of extension obtained from the McCoss construction according to the two average orientations. The orientation (3) corresponds to the strike of a hypothetical normal fault formed without influence of pre-existing structures according to the direction of extension.

mechanical stratigraphy in the study area. The Young's modulus of the Opalinus Clay is on average *c.* 10 GPa, in contrast to the much stiffer rocks constituting the underlying and overlying Muschelkalk and Malm interval respectively with Young's moduli of *c.* 40 GPa (Fig. 4). The Opalinus Clay has a low cohesion of 4 MPa and a low friction angle of 23° compared with the surrounding Malm and Muschelkalk with a cohesion greater than 20 MPa and a friction angle higher than 40°. In the study area, a maximum temperature of *c.* 85°C for the Opalinus Clay was reached during the Cretaceous for a depth of 1050 m, and a maximum burial depth of 1650 m was reached during the Miocene for a temperature of *c.* 66°C (Mazurek *et al.* 2006). Considering the evidence for late Miocene to recent erosion of *c.* 1000 m in the region of the northern Molasse Basin (Mazurek *et al.* 2006; von Hagke *et al.* 2012) the measured rock properties probably do not equal those at the time of faulting (post-early Miocene) when the Molasse section overlying the faulted Mesozoic units was thicker. Nevertheless, the relative strength and competence contrasts between the various units are unlikely to have been significantly different, particularly as the Jurassic Opalinus Clay was already compacted at this time. The measured rock properties for the Opalinus Clay are therefore consistent with the seismic observations of widespread continuous deformation in this unit at the seismic scale.

Seismic mapping indicates that the sections above and below the Opalinus Clay are more likely to accommodate extension by discrete faulting than the Opalinus Clay. It is clear that the monoclinal folding in the Opalinus Clay is not a poorly resolved normal fault, as the wavelength of the monocline is up to 300 m (Fig. 6b) and adjacent sections demonstrate that faults are readily imaged across it elsewhere (e.g. Fig. 7b, section (1)). Borehole data, however, indicate that the Opalinus Clay is generally less prone to development of brittle structures at the small scale. In the Schlattingen-1 borehole located about 5 km NE of our study area, and already within the adjacent Hegau–Lake Constance graben system, the Opalinus Clay is almost devoid of fractures whereas fault zones, shear fractures and veins are recorded above and below (Mazurek *et al.* 2018). The preferential location of fractures in the Malm and Muschelkalk competent units relative to the Opalinus

Clay incompetent unit is in accordance with differential stresses that are higher in stiffer formations as suggested from numerical modelling of the studied sequence (Hergert *et al.* 2015). However, the Schlattingen-1 borehole is located outside any monoclinal structure, and therefore may not be representative of the fracture frequency occurring in the Wildensbuch Fault Zone. Fracture data from the closer Benken borehole also show low fracture densities in the Opalinus Clay, but a collection of sub-seismic-scale veins and shear fractures occurs within a narrow zone near 700 m depth (Fig. 3; Nagra 2001, and references therein). From an Opalinus Clay rock laboratory at Mont Terri, located *c.* 100 km west of our study area in a reverse fault regime, meso- and small-scale deformation of Opalinus Clay is also reported to be dominantly brittle (Laurich *et al.* 2017; Jaeggi *et al.* 2018). Consequently, the possibility that the broad monocline associated with the Wildensbuch Fault Zone is accommodated by displacement on a number of small faults that individually are below the limit of seismic resolution cannot be ruled out.

Structural inheritance and fault zone geometry

The Wildensbuch Fault Zone forms a left-stepping array of segments at the level of the Malm unit. The available outcrop data (Madritsch 2015; Egli *et al.* 2017) indicate that these are normal fault segments and fault geometries and displacements are consistent with normal offset. The en echelon arrangement of the segments suggests that they formed under the influence of an underlying basement structure. By comparing the overall trend of the fault zone (*c.* 090°) and the average strike of the segments within the zone (*c.* 125°), the McCoss construction (McCoss 1986; Worthington & Walsh 2017) can be used to derive the extension direction responsible for the formation of the segmented array; the resulting extension direction is *c.* 060° (Fig. 12d). This orientation is perpendicular to the trend of the Neuhausen Fault central segment (Fig. 11a) and the small-scale normal faults observed in the Tertiary sand (Fig. 2), and is consistent with previous field studies (Madritsch 2015; Egli *et al.* 2017) that report similar striking normal faults at surface invoking a NE–SW Miocene extension direction. We infer that the Neuhausen Fault and the Wildensbuch Fault Zone formed under the same Miocene extension and that the Wildensbuch Fault Zone localized above a pre-existing east–west basement structure. Although the seismic imaging within the basement does not allow such deeper structures to be clearly identified, a Permo-Carboniferous normal fault with this trend beneath the Wildensbuch Fault Zone is considered plausible from a regional geological perspective (Marchant *et al.* 2005; Madritsch *et al.* 2018).

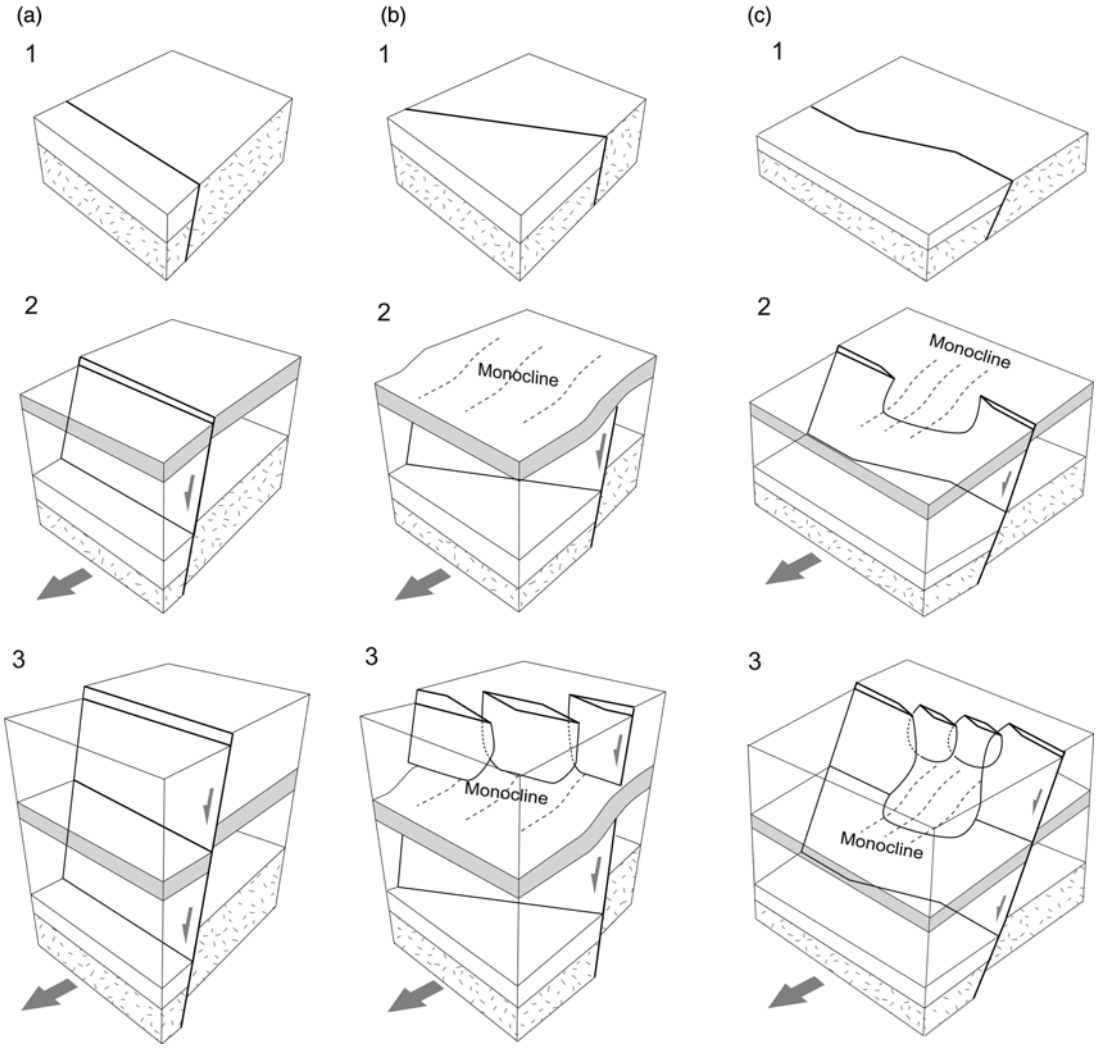

Fig. 13. Models of upward propagation of a pre-existing structure in a heterogeneous sequence. (**a**) The pre-existing structure is well oriented relative to the direction of extension, resulting in a continuous vertical propagation through the layered sequence. (**b**) The pre-existing structure is oblique relative to the stress field, resulting in the formation of a monocline in the less competent unit and the formation of an en echelon structure with segments striking with a different orientation than the pre-existing structure. (**c**) The pre-existing structure is locally oblique. In (**a**)–(**c**) 1, 2 and 3 are successive steps showing vertical propagation. For illustration, we represent a different portion of the sedimentary sequence in the different steps. The grey arrows represent the direction of extension at the time of reactivation. The grey layer corresponds to a less competent unit but continuous deformation extended above the layer.

Beneath the Opalinus Clay the individual fault segments strike *c.* 20° anticlockwise of those above (Fig. 5); that is, intermediate in orientation between the general trend of the Wildensbuch Fault Zone and the trend of the fault segments in the Malm unit. This strike change is attributed to upward bifurcation and twisting of the fault from a continuous basement fault at depth. Upward twisting of fault segments from a single reactivated basement structure has been described from seismic data (Giba *et al.* 2012) and is well known from analogue models of fault reactivation (Clifton *et al.* 2000; Corti 2008). In the case of the Wildensbuch Fault Zone this upward twisting is interrupted by the Opalinus Clay, across which there is a stepwise change in the strike of fault segments presumed to be due to mechanical decoupling across this weaker interval; similar stepwise changes in fault orientation are observed in reactivated fault systems in the presence of highly ductile salt units (Jackson & Rotevatn 2013).

The Neushausen Fault cutting through the Mesozoic section developed in response to Miocene extension. Egli *et al.* (2017) suggested that it also nucleated along a pre-existing basement structure trending parallel to it and perpendicular to the inferred Miocene extension direction (i.e. NW–SE). Hence it was not reactivated in an oblique manner as was the Wildensbuch Fault Zone. As mentioned previously, the Neuhausen eastern segment has an anomalous strike, forming a dog-leg in the otherwise continuous fault trace, and is aligned with the trace of the Wildensbuch Fault Zone (Fig. 1). We interpret that at this location, the Neuhausen Fault has locally followed the trace of the same roughly east–west-striking basement structure that lies beneath the Wildensbuch Fault Zone. This portion of the Neuhausen Fault does not seem to be segmented in the same way as the Wildensbuch Fault Zone but its location at the edge of the seismic dataset does not allow for a similarly detailed interpretation.

Model of formation of the fault zone under structural inheritance and layering control

In this section we discuss aspects of the development of the Wildensbuch Fault Zone that can be constrained by inspection of its displacement distribution. Whereas the degree of partitioning of the displacement into continuous and discontinuous components varies over the fault, with a locally significant continuous component within the Opalinus Clay, the distribution of the total displacement is largely unaffected by the Opalinus Clay and profiles of total displacement vary systematically, both along-strike and down-dip (Figs 9 and 10). Therefore, the various components of the fault array are all parts of a single coherent structure. In this context, monoclines seen on seismic lines act to transfer displacement between fault segments above and below (e.g. Fig. 10c) and are effectively dip relay zones between fault segments.

It could be considered that dip segmentation initially occurred along the entire length of the Wildensbuch Fault Zone and that the fault segments above and below the Opalinus Clay later established linkages at some locations to give the present-day 3D fault geometry (see Kattenhorn & Pollard 2001; Jackson & Rotevatn 2013; Lăpădat *et al.* 2017; Deng & McClay 2019). However, we do not consider this to be the case, partly because we do not see pronounced monocline development or overlapping fault segments, suggestive of pre-existing relay zones, associated with those parts of the Wildensbuch Fault Zone or the Neuhausen Fault that are continuous across the Opalinus Clay. Also, the total throw associated with continuous fault traces is not significantly larger than that associated with fault traces that are segmented in cross-section and so continuity is not established as throw increases, as would be expected if a continuous fault was established by linkage of dip relay zones. Instead, we favour a model in which the degree of segmentation of the fault across the Opalinus Clay reflects conditions during its initial propagation through the sequence and the fault propagated across the Opalinus Clay more readily at some locations than at others apparently depending on the fault orientation with respect to the direction of extension (Fig. 13). Faults that are continuous across the Opalinus Clay occur where the fault segments above and below the Opalinus Clay are parallel, suggesting that the fault was locally optimally oriented to propagate through the section. In contrast, in those areas where the fault is discontinuous across the Opalinus Clay, the segments above and below are oblique to one another, suggesting that the fault was not optimally oriented at the time of fault propagation, fault propagation was retarded by the Opalinus Clay, and a new and unconnected fault segment formed above the Opalinus Clay. In the case of the Wildensbuch Fault Zone, the orientations of these decoupled normal fault segments are compatible with the direction of Miocene extension.

Conclusions

The Wildensbuch Fault Zone is formed by oblique reactivation of a pre-existing basement structure that propagated upwards through a pronounced mechanically layered stratigraphy. Throw is transferred between fault segments both laterally and vertically via relay zones and open monoclines, so that a coherent displacement distribution is maintained even for segments that are widely separated in map view relative to their displacement. The unit of key importance for fault zone development is the Opalinus Clay, a weak claystone that is over- and underlain by much more competent rock units. Whereas the overlying and underlying units deformed in a brittle manner, the Opalinus Clay commonly deformed in a largely continuous manner resulting in open monoclines. However, folding is by no means ubiquitous and despite its relatively low Young's modulus and failure angle, faults can be continuous across the Opalinus Clay on both the Wildensbuch Fault Zone and the related Neuhausen Fault with little or no continuous deformation. Folding is most pronounced when fault segments above and below the Opalinus Clay Formation have oblique strike to each other and is much reduced to absent when the fault has the same strike above and below the Opalinus Clay. Therefore, the impact of an incompetent unit such as the Opalinus Clay on the geometry of fault zones is not simply a function of the mechanical contrast at the time of faulting but is also a function of the orientation of the fault zone to the extension direction. Increasing obliquity to the extension direction (e.g. owing to reactivation of precursor structure) favours fault segmentation across such units, which show a tendency to deform in a continuous instead of discontinuous manner, whereas faults striking perpendicular to extension may show no segmentation despite a strong mechanical contrast within sedimentary layering.

Acknowledgements Fault analyses were performed using TrapTester (Badley Earth Science) and Move software (Midland Valley). We thank the members of the Fault Analysis Group and Silvio Gige for many useful discussions on this topic, and D. Ferrill and C. Nussbaum for useful reviews of the paper.

Funding This research was supported by Nagra (Swiss National Cooperative for the Disposal of Radioactive Waste) and by a consortium-sponsored project brokered by the Industry Technology Facilitator, and funded by Anadarko, ConocoPhillips (UK), Eni, ExxonMobil, Equinor, Shell, Total E&P UK and Woodside Energy. C. Childs is funded by Tullow Oil. This publication benefited from research supported in part by a research grant from Science Foundation Ireland (SFI) under Grant Number 13/RC/2092 and co-funded under the European Regional Development Fund and by PIPCO RSG and its member companies.

Author contributions VR: Conceptualization (Lead), Formal analysis (Lead), Investigation (Lead), Methodology (Lead), Writing – Original Draft (Lead); CC: Conceptualization (Equal), Methodology (Equal), Supervision (Lead), Writing – Original Draft (Equal), Writing – Review & Editing (Equal); HM: Resources (Lead), Writing – Review & Editing (Equal); GC:

Conceptualization (Supporting), Formal analysis (Supporting), Investigation (Supporting), Methodology (Supporting)

Scientific editing by Karel Schulmann

References

Agosta, F., Wilson, C. & Aydin, A. 2015. The role of mechanical stratigraphy on normal fault growth across a Cretaceous carbonate multi-layer, central Texas (USA). *Italian Journal of Geosciences*, **134**, 423–441, https://doi.org/10.3301/IJG.2014.20

Baudon, C. & Cartwright, J. 2008. Early stage evolution of growth faults: 3D seismic insights from the Levant Basin, Eastern Mediterranean. *Journal of Structural Geology*, **30**, 888–898, https://doi.org/10.1016/j.jsg.2008.02.019

Birkhäuser, P., Roth, P., Meier, B. & Naef, H. 2001. *3D-Seismik: Räumliche Erkundung der mesozoischen Sedimentschichten im Zürcher Weinland*. Nagra Technical Report, **NTB 00-03**. Nagra, Wettingen.

Burkhard, M. 1990. Aspects of the large-scale Miocene deformation in the most external part of the Swiss Alps (sub-Alpine molasse to Jura fold belt). *Eclogae Geologicae Helvetiae*, **83**, 559–583.

Camanni, G., Roche, V. *et al.* 2019. The three-dimensional geometry of relay zones within segmented normal faults. *Journal of Structural Geology*, **129**, 103895, https://doi.org/10.1016/j.jsg.2019.103895

Childs, C., Watterson, J. & Walsh, J.J. 1995. Fault overlap zones within developing normal fault systems. *Journal of the Geological Society, London*, **152**, 535–549, https://doi.org/10.1144/gsjgs.152.3.0535

Childs, C., Nicol, A., Walsh, J.J. & Watterson, J. 1996. Growth of vertically segmented normal faults. *Journal of Structural Geology*, **18**, 1389–1397, https://doi.org/10.1016/S0191-8141(96)00060-0

Childs, C., Manzocchi, T., Nicol, A., Walsh, J.J., Soden, A.M., Conneally, J.C. & Delogkos, E. 2017. The relationship between normal drag, relay ramp aspect ratio and fault zone structure. *In*: Childs, C., Holdsworth, R.E., Jackson, C.A.-L., Manzocchi, T., Walsh, J.J. & Yielding, G. (eds) *The Geometry and Growth of Normal Faults*. Geological Society, London, Special Publications, **439**, 355–372, https://doi.org/10.1144/SP439.16

Clifton, A.E., Schlische, R.W., Withjack, M.O. & Ackermann, R.V. 2000. Influence of rift obliquity on fault-population systematics: results of experimental clay models. *Journal of Structural Geology*, **22**, 1491–1509, https://doi.org/10.1016/S0191-8141(00)00043-2

Conneally, J., Childs, C. & Nicol, A. 2017. Monocline formation during growth of segmented faults in the Taranaki Basin, offshore New Zealand. *Tectonophysics*, **721**, 310–321, https://doi.org/10.1016/j.tecto.2017.06.036

Corbett, K., Friedman, M. & Spang, J. 1987. Fracture development and mechanical stratigraphy of Austin Chalk, Texas. *AAPG Bulletin*, **71**, 17–28.

Corti, G. 2008. Control of rift obliquity on the evolution and segmentation of the main Ethiopian rift. *Nature Geoscience*, **1**, 258–264, https://doi.org/10.1038/ngeo160

Delogkos, E., Manzocchi, T. *et al.* 2017. Throw partitioning across normal fault zones in the Ptolemais Basin, Greece. *In*: Childs, C., Holdsworth, R.E., Jackson, C.A.-L., Manzocchi, T., Walsh, J.J. & Yielding, G. (eds) *The Geometry and Growth of Normal Faults*. Geological Society, London, Special Publications, **439**, 333–353, https://doi.org/10.1144/SP439.19

Deng, H. & McClay, K. 2019. Development of extensional fault and fold system: Insights from 3D seismic interpretation of the Enderby Terrace, NW Shelf of Australia. *Marine and Petroleum Geology*, **104**, 11–28, https://doi.org/10.1016/j.marpetgeo.2019.03.003

Diebold, P. & Noack, T. 1997. Late Paleozoic troughs and Tertiary structures in the eastern folded Jura. *In*: Pfiffner, O.A. *et al.* (eds) *Deep Structure of the Swiss Alps–Results From NRP 20*, Birkhäuser Boston, Cambridge, MA. **20**, 59–63.

Echtler, H.P. & Chauvet, A. 1992. Carboniferous convergence and subsequent crustal extension in the southern Schwarzwald (SW Germany). *Geodinamica Acta*, **5**, 37–49, https://doi.org/10.1080/09853111.1992.11105218

Egli, D., Mosar, J., Ibele, T. & Madritsch, H. 2017. The role of precursory structures on Tertiary deformation in the Black Forest–Hegau region. *International Journal of Earth Sciences*, **106**, 2297–2318, https://doi.org/10.1007/s00531-016-1427-8

Eisbacher, G.H., Lüschen, E. & Wickert, F. 1989. Crustal-scale thrusting and extension in the Hercynian Schwarzwald and Vosges, central Europe. *Tectonics*, **8**, 1–21, https://doi.org/10.1029/TC008i001p00001

Ferrill, D.A. & Morris, A.P. 2003. Dilational normal faults. *Journal of Structural Geology*, **25**, 183–196, https://doi.org/10.1016/S0191-8141(02)00029-9

Ferrill, D.A. & Morris, A.P. 2008. Fault zone deformation controlled by carbonate mechanical stratigraphy, Balcones fault system, Texas. *AAPG Bulletin*, **92**, 359–380, https://doi.org/10.1306/10290707066

Ferrill, D.A., Sims, D.W., Waiting, D.J., Morris, A.P., Franklin, N.M. & Schultz, A.L. 2004. Structural framework of the Edwards Aquifer recharge zone in south–central Texas. *Geological Society of America Bulletin*, **116**, 407–418, https://doi.org/10.1130/B25174.1

Ferrill, D.A., Morris, A.P., Sims, D.W., Waiting, D.J. & Hasegawa, S. 2005. Development of synthetic layer dip adjacent to normal faults. *In*: Sorkhabi, R. & Tsuji, Y. (eds) *Faults, Fluid Flow, and Petroleum Traps*. AAPG Memoirs, **85**, 125–138.

Ferrill, D.A., Morris, A.P., McGinnis, R.N., Smart, K.J. & Ward, W.C. 2011. Fault zone deformation and displacement partitioning in mechanically layered carbonates: The Hidden Valley fault, central Texas. *AAPG Bulletin*, **95**, 1383–1397, https://doi.org/10.1306/12031010065

Ferrill, D.A., Morris, A.P., McGinnis, R.N., Smart, K.J., Wigginton, S.S. & Hill, N.J. 2017. Mechanical stratigraphy and normal faulting. *Journal of Structural Geology*, **94**, 275–302, https://doi.org/10.1016/j.jsg.2016.11.010

Geyer, O.F., Gwinner, M.P., Geyer, M., Nitsch, E. & Simon, T. 2011. *Geologie von Baden-Württemberg*. Schweizerbart, Stuttgart.

Giba, M., Walsh, J.J. & Nicol, A. 2012. Segmentation and growth of an obliquely reactivated normal fault. *Journal of Structural Geology*, **39**, 253–267, https://doi.org/10.1016/j.jsg.2012.01.004

Giger, S. & Marschall, P. 2014. *Geomechanical properties, rock models and in-situ stress conditions for Opalinus Clay in Northern Switzerland*. Nagra Working Report, **NAB 14-01**. Nagra, Wettingen.

Grant, J.V. & Kattenhorn, S.A. 2004. Evolution of vertical faults at an extensional plate boundary, southwest Iceland. *Journal of Structural Geology*, **26**, 537–557, https://doi.org/10.1016/j.jsg.2003.07.003

Hergert, T., Heidbach, O., Reiter, K., Giger, S.B. & Marschall, P. 2015. Stress field sensitivity analysis in a sedimentary sequence of the Alpine foreland, northern Switzerland. *Solid Earth*, **6**, 533–552, https://doi.org/10.5194/se-6-533-2015

Hinsken, S., Ustaszewski, K. & Wetzel, A. 2007. Graben width controlling syn-rift sedimentation: the Palaeogene southern Upper Rhine Graben as an example. *International Journal of Earth Sciences*, **96**, 979–1002, https://doi.org/10.1007/s00531-006-0162-y

Hofmann, F., Schlatter, R. & Weh, M. 2000. *Erläuterungen zum Blatt 1011 Beggingen (Südhälfte) mit SW-Anteil von Blatt 1012 Singen. Geologischer Atlas der Schweiz, 1:25.000*.

Homberg, C., Schnyder, J., Roche, V., Leonardi, V. & Benzaggagh, M. 2017. The brittle and ductile components of displacement along fault zones. *In*: Childs, C., Holdsworth, R.E., Jackson, C.A.-L., Manzocchi, T., Walsh, J.J. & Yielding, G. (eds) *The Geometry and Growth of Normal Faults*. Geological Society, London, Special Publications, **439**, 395–412, https://doi.org/10.1144/SP439.21

Jackson, C.A.L. & Rotevatn, A. 2013. 3D seismic analysis of the structure and evolution of a salt-influenced normal fault zone: a test of competing fault growth models. *Journal of Structural Geology*, **54**, 215–234, https://doi.org/10.1016/j.jsg.2013.06.012

Jackson, C.A.L., Gawthorpe, R.L. & Sharp, I.R. 2006. Style and sequence of deformation during extensional fault-propagation folding: examples from the Hammam Faraun and El-Qaa fault blocks, Suez Rift, Egypt. *Journal of Structural Geology*, **28**, 519–535, https://doi.org/10.1016/j.jsg.2005.11.009

Jaeggi, D., Laurich, B., Nussbaum, C., Schuster, K. & Connolly, P. 2018. Tectonic structure of the 'Main Fault' in the Opalinus Clay, Mont Terri rock laboratory (Switzerland). *In*: Bossart, P. & Milnes, A. (eds) Mont Terri Rock Laboratory, 20 Years. *Swiss Journal of Geosciences*, Supplement, vol 5. Birkhäuser, Cham, 68–86.

Jordan, P., Malz, A., Heuberger, S., Pietsch, J., Kley, J. & Madritsch, H. 2015. *Regionale geologische Profilschnitte durch die Nordschweiz und 2D-Bilanzierung der Fernschubdeformation im östlichen Faltenjura: Arbeitsbericht zu SGT Etappe 2*. Nagra Arbeitsbericht, **NAB 14**. Nagra, Wettingen.

Jordan, P., Pietsch, J.S. *et al.* 2016. The middle to late Triassic Bänkerjoch and Klettgau formations of northern Switzerland. *Swiss Journal of Geosciences*, **109**, 257–284, https://doi.org/10.1007/s00015-016-0218-3

Kattenhorn, S.A. & Pollard, D.D. 2001. Integrating 3-D seismic data, field analogs, and mechanical models in the analysis of segmented normal faults in the Wytch Farm oil field, southern England, United Kingdom. *AAPG Bulletin*, **85**, 1183–1210, https://doi.org/10.1306/8626CA91-173B-11D7-8645000102C1865D

Kempf, O. & Pfiffner, O.A. 2004. Early Tertiary evolution of the North Alpine Foreland Basin of the Swiss Alps and adjoining areas. *Basin Research*, **16**, 549–567, https://doi.org/10.1111/j.1365-2117.2004.00246.x

Lăpădat, A., Imber, J., Yielding, G., Iacopini, D., McCaffrey, K.J., Long, J.J. & Jones, R.R. 2017. Occurrence and development of folding related to normal faulting within a mechanically heterogeneous sedimentary sequence: a case study from Inner Moray Firth, UK. *In*: Childs, C., Holdsworth, R.E., Jackson, C.A.-L., Manzocchi, T., Walsh, J.J. & Yielding, G. (eds) *The Geometry and Growth of Normal Faults*. Geological Society, London, Special Publications, **439**, 373–394, https://doi.org/10.1144/SP439.18

Laubach, S.E., Olson, J.E. & Gross, M.R. 2009. Mechanical and fracture stratigraphy. *AAPG Bulletin*, **93**, 1413–1426, https://doi.org/10.1306/07270909094

Laurich, B., Urai, J.L. & Nussbaum, C. 2017. Microstructures and deformation mechanisms in Opalinus Clay: Insights from scaly clay from the Main Fault in the Mont Terri Rock Laboratory (CH). *Solid Earth*, **8**, 27–44, https://doi.org/10.5194/se-8-27-2017

Madritsch, H. 2015. Outcrop-scale fracture systems in the Alpine foreland of central northern Switzerland: kinematics and tectonic context. *Swiss Journal of Geosciences*, **108**, 155–181, https://doi.org/10.1007/s00015-015-0203-2

Madritsch, H., Naef, H., Meier, B., Franzke, H.J. & Schreurs, G. 2018. Architecture and kinematics of the Constance–Frick Trough (Northern Switzerland): implications for the formation of post-Variscan basins in the foreland of the Alps and scenarios of their Neogene reactivation. *Tectonics*, **37**, 2197–2220, https://doi.org/10.1029/2017TC004945

Mansfield, C.S. & Cartwright, J.A. 1996. High resolution fault displacement mapping from three-dimensional seismic data: evidence for dip linkage during fault growth. *Journal of Structural Geology*, **18**, 249–263, https://doi.org/10.1016/S0191-8141(96)80048-4

Marchant, R., Ringgenberg, Y., Stampfli, G., Birkhäuser, P., Roth, P. & Meier, B. 2005. Paleotectonic evolution of the Zürcher Weinland (northern Switzerland), based on 2D and 3D seismic data. *Eclogae Geologicae Helvetiae*, **98**, 345–362, https://doi.org/10.1007/s00015-005-1171-8

Mazurek, M., Hurford, A.J. & Leu, W. 2006. Unravelling the multi-stage burial history of the Swiss Molasse Basin: integration of apatite fission track, vitrinite reflectance and biomarker isomerisation analysis. *Basin Research*, **18**, 27–50, https://doi.org/10.1111/j.1365-2117.2006.00286.x

Mazurek, M., Davis, D.W., Madritsch, H., Rufer, D., Villa, I.M., Sutcliffe, C.N. & Traber, D. 2018. Veins in clay-rich aquitards as records of deformation and fluid-flow events in northern Switzerland. *Applied Geochemistry*, **95**, 57–70, https://doi.org/10.1016/j.apgeochem.2018.05.010

McCoss, A.M. 1986. Simple constructions for deformation in transpression/transtension zones. *Journal of Structural Geology*, **8**, 715–718, https://doi.org/10.1016/0191-8141(86)90077-5

Meier, B., Kuhn, P., Roth, P. & Madritsch, H. 2014. *Tiefenkonvertierung der regionalen Strukturinterpretation der Nagra 2D-Seismik 2011/12*. Nagra Working Report, **NAB 14-34**. Nagra, Wettingen.

Morris, A.P., Ferrill, D.A. & McGinnis, R.N. 2009. Mechanical stratigraphy and faulting in Cretaceous carbonates. *AAPG Bulletin*, **93**, 1459–1470, https://doi.org/10.1306/04080909011

Müller, W.H., Naef, H. & Graf, H.R. 2002. *Geologische Entwicklung der Nordschweiz, Neotektonik und Langzeitszenarien Zürcher Weinland*. Nagra, Wettingen.

Muraoka, H. & Kamata, H. 1983. Displacement distribution along minor fault traces. *Journal of Structural Geology*, **5**, 483–495, https://doi.org/10.1016/0191-8141(83)90054-8

Nagra 2001. *Sondierbohrung Benken – Untersuchungsbericht*. Nagra Technischer Bericht, **NTB 00-01**. Nagra, Wettingen.

Nagra 2014. SGT Etappe 2: Vorschlag weiter zu untersuchender geologischer Standortgebiete mit zugehörigen Standortarealen für die Oberflächenanlage: Geologische Grundlagen / Dossier II. Nagra Technical Report NTB 14-02. Wettingen, Nagra.

Peacock, D.C.P. & Sanderson, D.J. 1991. Displacements, segment linkage and relay ramps in normal fault zones. *Journal of Structural Geology*, **13**, 721–733, https://doi.org/10.1016/0191-8141(91)90033-F

Peacock, D.C.P. & Sanderson, D.J. 1992. Effects of layering and anisotropy on fault geometry. *Journal of the Geological Society, London*, **149**, 793–802, https://doi.org/10.1144/gsjgs.149.5.0793

Peacock, D.C.P. & Zhang, X. 1994. Field examples and numerical modelling of oversteps and bends along normal faults in cross-section. *Tectonophysics*, **234**, 147–167, https://doi.org/10.1016/0040-1951(94)90209-7

Pfiffner, O.A. 1986. Evolution of the north Alpine foreland basin in the Central Alps. *In*: Allen, P.A. & Homewood, P. (eds) *Foreland Basins*. International Association of Sedimentologists, Special Publications, **8**, 219–228.

Roche, V. & Van der Baan, M. 2015. The role of lithological layering and pore pressure on fluid-induced microseismicity. *Journal of Geophysical Research: Solid Earth*, **120**, 923–943, https://doi.org/10.1002/2014JB011606

Roche, V., Homberg, C. & Rocher, M. 2012. Fault displacement profiles in multilayer systems: from fault restriction to fault propagation. *Terra Nova*, **24**, 499–504, https://doi.org/10.1111/j.1365-3121.2012.01088.x

Roche, V., Homberg, C., David, C. & Rocher, M. 2014. Normal faults, layering and elastic properties of rocks. *Tectonophysics*, **622**, 96–109, https://doi.org/10.1016/j.tecto.2014.03.006

Roche, V., Homberg, C., van der Baan, M. & Rocher, M. 2017. Widening of normal fault zones due to the inhibition of vertical propagation. *In*: Childs, C., Holdsworth, R.E., Jackson, C.A.-L., Manzocchi, T., Walsh, J.J. & Yielding, G. (eds) *The Geometry and Growth of Normal Faults*. Geological Society, London, Special Publications, **439**, 271–288, https://doi.org/10.1144/SP439.5

Saqab, M.M. & Bourget, J. 2015. Structural style in a young flexure-induced oblique extensional system, north-western Bonaparte Basin, Australia. *Journal of Structural Geology*, **77**, 239–259, https://doi.org/10.1016/j.jsg.2015.06.002

Schreiner, A. 1992. *Hegau und westlicher Bodensee. Geologische. Karte von Baden-Württemberg 1:50 000, Erläuterungen*.

Sinclair, H.D. & Allen, P.A. 1992. Vertical versus horizontal motions in the Alpine orogenic wedge: stratigraphic response in the foreland basin. *Basin Research*, **4**, 215–232, https://doi.org/10.1111/j.1365-2117.1992.tb00046.x

Sommaruga, A., Mosar, J., Schori, M. & Gruber, M. 2017. The role of the Triassic evaporites underneath the North Alpine Foreland. *In*: Soto, J.I., Flinch, J.F. & Tari, G. (eds) *Permo-Triassic Salt Provinces of Europe, North Africa and the Atlantic Margins*, Elsevier, Amsterdam, 447–466.

Tvedt, A.B., Rotevatn, A., Jackson, C.A.L., Fossen, H. & Gawthorpe, R.L. 2013. Growth of normal faults in multilayer sequences: a 3D seismic case study from the Egersund Basin, Norwegian North Sea. *Journal of Structural Geology*, **55**, 1–20, https://doi.org/10.1016/j.jsg.2013.08.002

Vasquez, L., Nalpas, T., Ballard, J.F., Veslud, C.L.C.D., Simon, B., Dauteuil, O. & Bernard, X.D. 2018. 3D geometries of normal faults in a brittle–ductile sedimentary cover: Analogue modelling. *Journal of Structural Geology*, **112**, 29–38, https://doi.org/10.1016/j.jsg.2018.04.009

von Hagke, C., Cederbom, C.E., Oncken, O., Stöckli, D.F., Rahn, M.K. & Schlunegger, F. 2012. Linking the northern Alps with their foreland: the latest exhumation history resolved by low temperature thermochronology. *Tectonics*, **31**, TC5010, https://doi.org/10.1029/2011TC003078

Wetzel, A., Allenbach, R. & Allia, V. 2003. Reactivated basement structures affecting the sedimentary facies in a tectonically "quiescent" epicontinental basin: an example from NW Switzerland. *Sedimentary Geology*, **157**, 153–172, https://doi.org/10.1016/S0037-0738(02)00230-0

Wilkins, S.J. & Gross, M.R. 2002. Normal fault growth in layered rocks at Split Mountain, Utah: influence of mechanical stratigraphy on dip linkage, fault restriction and fault scaling. *Journal of Structural Geology*, **24**, 1413–1429, https://doi.org/10.1016/S0191-8141(01)00154-7

Willett, S.D. & Schlunegger, F. 2010. The last phase of deposition in the Swiss Molasse Basin: from foredeep to negative-alpha basin. *Basin Research*, **22**, 623–639, https://doi.org/10.1111/j.1365-2117.2009.00435.x

Wilson, P., Elliott, G.M., Gawthorpe, R.L., Jackson, C.A.L., Michelsen, L. & Sharp, I.R. 2013. Geometry and segmentation of an evaporite-detached normal fault array: 3D seismic analysis of the southern Bremstein Fault Complex, offshore mid-Norway. *Journal of Structural Geology*, **51**, 74–91, https://doi.org/10.1016/j.jsg.2013.03.005

Worthington, R.P. & Walsh, J.J. 2017. Timing, growth and structure of a reactivated basin-bounding fault. *In*: Childs, C., Holdsworth, R.E., Jackson, C.A.-L., Manzocchi, T., Walsh, J.J. & Yielding, G. (eds) *The Geometry and Growth of Normal Faults*. Geological Society, London, Special Publications, **439**, 511–531, https://doi.org/10.1144/SP439.14

Ziegler, P.A. 1992. European Cenozoic rift system. *Tectonophysics*, **208**, 91–111, https://doi.org/10.1016/0040-1951(92)90338-7